DOI: 10.1002/chem.200902527

Dihydronaphthalene-Fused Boron–Dipyrromethene (BODIPY) Dyes: Insight into the Electronic and Conformational Tuning Modes of BODIPY Fluorophores

Yan-Wei Wang,[a] Ana B. Descalzo,[b] Zhen Shen,*[a] Xiao-Zeng You,[a] and Knut Rurack*[b]

Abstract: A new series of boron–dipyrromethene (BDP, BODIPY) dyes with dihydronaphthalene units fused to the β-pyrrole positions (**1a**–**d**, **2**) has been synthesised and spectroscopically investigated. All the dyes, except pH-responsive **1d** in polar solvents, display intense emission between 550–700 nm. Compounds **1a** and **1b** with a hydrogen atom and a methyl group in the *meso* position of the BODIPY core show spectroscopic properties that are similar to those of rhodamine 101, thus rendering them potent alternatives to the positively charged rhodamine dyes as stains and labels for less polar environments or for the dyeing of latex beads. Compound **1d**, which carries an electron-donating 4-(dimethylamino)-phenyl group in the *meso* position, shows dual fluorescence in solvents more polar than dibutyl ether and can act as a pH-responsive "light-up" probe for acidic pH. Correlation of the pK_a data of **1d** and several other *meso*-(4-dimethylanilino)-substituted BODIPY derivatives allowed us to draw conclusions on the influence of steric crowding at the *meso* position on the acidity of the aniline nitrogen atom. Preparation and investigation of **2**, which carries a nitrogen instead of a carbon as the *meso*-bridgehead atom, suggests that the rules of colour tuning of BODIPYs as established so far have to be reassessed; for all the reported couples of *meso*-C- and *meso*-N-substituted BODIPYs, the exchange leads to pronounced redshifts of the spectra and reduced fluorescence quantum yields. For **2**, when compared with **1a**, the opposite is found: negligible spectral shifts and enhanced fluorescence. Additional X-ray crystallographic analysis of **1a** and quantum chemical modelling of the title and related compounds employing density functional theory granted further insight into the features of such sterically crowded chromophores.

Keywords: boron · dyes/pigments · fluorescent probes · photophysics · protonation

Introduction

Boron–dipyrromethene dyes (Scheme 1), also known as BDP or BODIPY dyes, are a class of widely used fluoro-

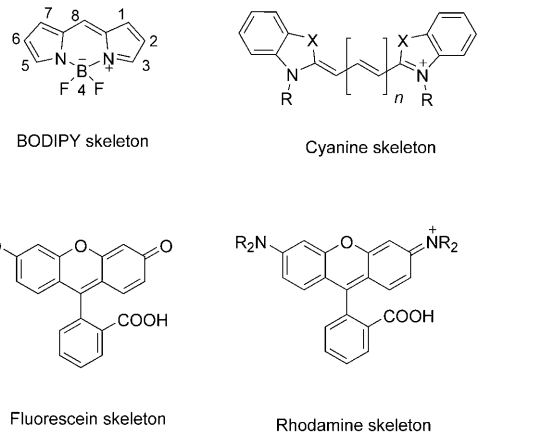

Scheme 1. Skeleton structures of selected popular chromophores for optical applications in bio-, materials and analytical chemistry; for BODIPYs, the 8-position of the dipyrrin core corresponds to the *meso* position; for cyanines, commonly $n=0$, 1, 2 and $X=C(CH_3)_2$, O, S.

[a] Y.-W. Wang, Prof. Z. Shen, Prof. X.-Z. You
State Key Laboratory of Coordination Chemistry
Nanjing National Laboratory of Microstructures
School of Chemistry and Chemical Engineering
Nanjing University, Nanjing 210093 (China)
Fax: (+86) 25-8331-4502
E-mail: zshen@nju.edu.cn

[b] Dr. A. B. Descalzo, Dr. K. Rurack
Fachgruppe I.5, BAM Bundesanstalt
für Materialforschung und -prüfung
Richard-Willstätter-Strasse 11, 12489 Berlin (Germany)
Fax: (+49) 30-8104-1157
E-mail: knut.rurack@bam.de

Supporting information for this article is available on the WWW under http://dx.doi.org/10.1002/chem.200902527.

phores.[1–6] They became very popular as laser dyes, fluorescent stains and labels in fluorescence imaging and as indicator dyes in sensory applications. Today, at least as judged by the rapidly growing number of reports,[7] their popularity is still growing, presumably because of their advantageous spectroscopic properties and considerably high photostability. BODIPYs are also frequent building blocks in molecular optoelectronic devices, energy-transfer cascades or multimode switches.[8–13] The literature on syntheses of new BODIPYs and their properties is abundant. Simple, alkyl-substituted dipyrrin BODIPYs, however, display absorption and emission bands with maxima only in the region of 480–540 nm so that today considerable effort is being made to shift the optical properties to the red.[5,14–18] Several strategies have been reported to be successful such as the introduction of aryl substituents in the 3,5- and/or 1,7-positions of the BODIPY core (like in compounds **4**,[19] **5**,[20] **6**,[21] **7**,[22] **8**[23] and **9**;[24] Scheme 2) or electron acceptors in the *meso* position,[25–27] aromatic ring fusion,[28–30] extension of the electronic π system by styryl substitution[31–38] or aza-substitution of the *meso*-carbon atom (like in compounds **7** and **9**; Scheme 2).

BODIPY dyes can be seen as rigid, cross-conjugated cyanines, and the majority of BODIPYs have been developed to complement or substitute classical fluorophores such as fluoresceins and rhodamines, which fluoresce in the visible range. The BODIPY core principally combines the advantageous properties of cyanines such as high molar absorption coefficients (ε_λ) and narrow band shapes with high fluorescence yields, typically $\Phi_f > 50\,\%$. In addition to an increased brightness, the product $\varepsilon_\lambda \times \Phi_f$, the difference to most cyanines is that cyanines are normally less photo- and chemically stable. Moreover, compared with the positively charged cyanine and rhodamine dyes and the negatively charged fluoresceins,[39] BODIPYs are zwitterionic molecules (Scheme 1), thereby rendering them ideally suitable for a broad range of solvents and environments (e.g., sensor matrices) of different polarity and pH. In addition, most BODIPYs are sufficiently water soluble at concentrations relevant for biochemical or analytical applications. The higher lipophilicity of the BODIPYs makes them ideal candidates for the dyeing of polymer particles and for the study of less polar environments.[21,30,40–43]

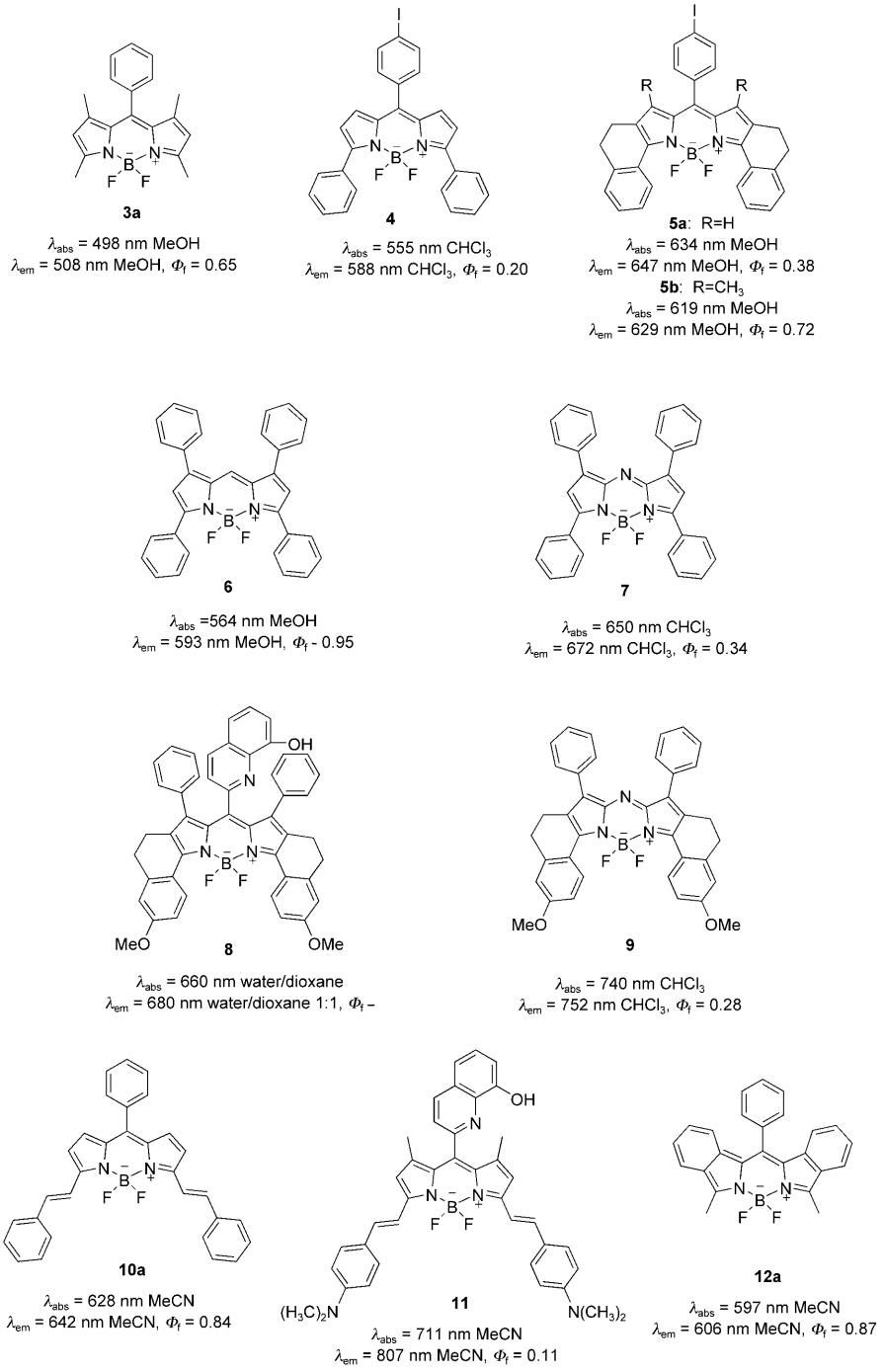

Scheme 2. Chemical structures of BODIPY dyes from the literature discussed here.

Besides favourable spectroscopic performance and solubility properties, the versatility of the BODIPY core with respect to functionalisation contributes especially to the popularity of the dyes. A comparison of the parent BODIPY skeleton in Scheme 1 with the selection of dyes shown in Scheme 2 shows that all seven of the numbered carbon atoms of the dipyrrin core are readily accessible to the introduction of substituents. Furthermore, the exchange of the two fluorine atoms at the boron centre is also possible, thus opening up even more routes to the chemical functionalisation of these dyes.[44] Concerning the development of functional, that is, addressable and analyte-responsive BODIPY dyes, the introduction of a substituent at the *meso* position is synthetically the most obvious and usually least demanding strategy and often results in compounds that show optimum performance with respect to fluorescence switching, at least when BODIPY core and *meso* group are perpendicularly oriented, that is, electronically virtually decoupled.[45,46] On the other hand, the simplest way to obtain BODIPYs with emission in the red-visible or near infrared (NIR) region of the spectrum is the condensation of 4-donor-substituted benzaldehydes to the active methyl groups located at the 3,5-positions of the BODIPY core.[31,35,47–49] The following rules of thumb for bathochromic displacement along this route can be derived from the data in Scheme 2 with tetramethyl-BODIPY **3a** serving as the reference for the parent dipyrrin chromophore:[50]

1) Introduction of two phenyl groups at the 3,5-positions entails a shift of approximately 50 nm (**3a**→**4**).
2) Introduction of two styryl groups at the 3,5-positions entails a shift of approximately 100 nm (**3a**→**10a**).
3) Introduction of two 4-dimethylaminostyryl groups at the 3,5-positions entails a shift of approximately 200 nm (**3a**→**11**).

Alternatively, the other strategies apparent from Scheme 2 lead to the following shifts:

1) Introduction of two phenyl groups at the 1,7-positions entails a shift of approximately 10 nm (**4**→**6**).
2) Rigidisation of two 3,5-phenyl groups, which is equivalent to the fusion of two dihydronaphthalene groups to the core, entails a shift of approximately 100 nm, along with a beneficial increase in Φ_f (**4**→**5a**).
3) Exchange of the *meso*-carbon atom for a nitrogen atom entails a shift of approximately 100 nm (**6**→**7** and **8**→**9**).

In taking into account these colour rules, one arrives at the conclusion that for a BODIPY dye that has the *meso* position still available for further functionalisation with an addressable unit, the introduction of styryl groups to the 3,5-positions and a rigidisation of additionally appended phenyl rings at the 1,7-position might finally yield potent NIR chromophores. With procedures for 3,5-BODIPY functionalisation being well established, even for ring-fused BODIPYs,[35] the key task toward such compounds is the introduction of bridged phenyl groups in the 1,7-position, that is, the fusion of dihydronaphthalene groups (with their 1,2-positions) to the 1,2- and 6,7-positions of the BODIPY core. Based on our experience in the synthesis of ring-fused BODIPYs,[29,30] we embarked on the synthesis and present here the preparation and spectroscopic properties of the newly designed dihydronaphthalene-appended BODIPY dyes **1a–d** and **2** (Scheme 3). Since the dihydrobenzo[*e*]-

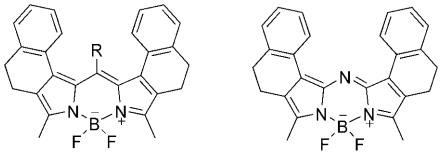

1a: R = H
1b: R = CH_3
1c: R = C_6H_5
1d: R = *p*-Me_2N-C_6H_4

2

Scheme 3. Chemical structures of the boron dihydrobenzo[*e*]isoindole or dihydronaphthalene-BODIPY dyes.

isoindole moieties in **1** and **2** lead to pronounced steric crowding at the *meso* position, we deliberately varied the nature of the substituent at the *meso* position from less demanding (H in **1a**) through moderately (CH_3 in **1b**) to strongly demanding (phenyl in **1c**,**d**) as well as the nature of the *meso* atom itself (from C in **1** to N in **2**) to get a better understanding of the tuning modes of BODIPY dyes. Synthesis of the pH-sensitive dye **1d** was conducted to study the influence of the novel BODIPY framework on an addressable *meso* group.

Results and Discussion

Synthesis: The corresponding BODIPY derivatives **1a–d** and **2** were prepared as shown in Scheme 4. Compound **1a** was obtained as a byproduct in the reaction to both the precursors of **1c** and **1d**. The precursor of **1c** was obtained by condensation of compound **I**[51] and benzaldehyde in the presence of trifluoroacetic acid (TFA). Then, 2,3-dichloro-5,6-dicyano-1,4-benzoquinone (DDQ) was added. The precursor of **1d** was prepared in the same way from 4-(dimethylamino)benzaldehyde. The precursor of **1b** was prepared by condensation of **I** with acetyl chloride. Finally, for the precursor of **2**, **I** was reacted with $NaNO_2$ in a mixture of AcOH/Ac_2O. To obtain the final BODIPY dyes, the boron difluoride bridge was subsequently introduced in all cases by treatment of the corresponding dipyrrin derivatives with boron trifluoride diethyl etherate (BF_3·Et_2O) in the presence of triethylamine (TEA) to yield compounds **1a–d** and **2**, which were purified by column chromatography on silica gel and further recrystallisation in chloroform/methanol mixtures.

Crystal structure of 1a: Although a transfer of structural properties from the solid state to solution can serve only as

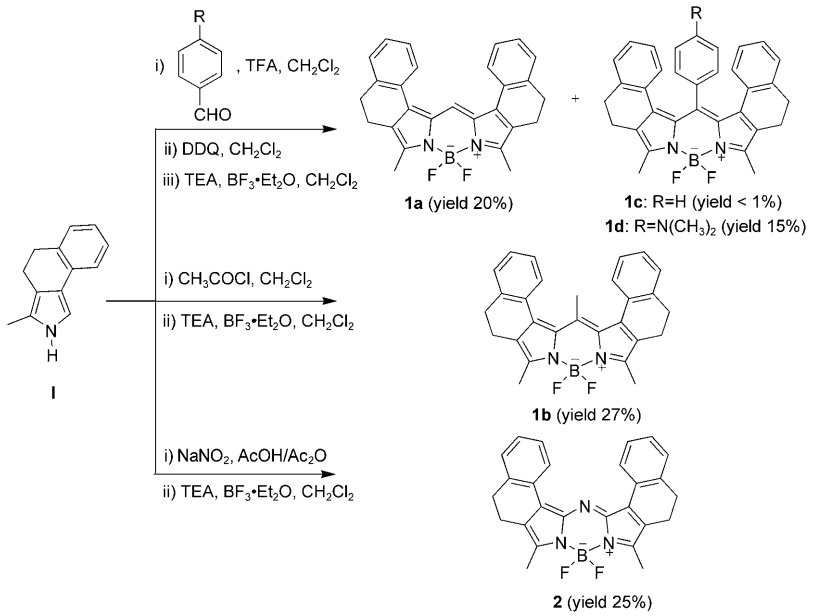

Scheme 4. Synthetic routes to compounds **1a–d** and **2**.

a first approximation, especially for conformationally highly constrained compounds such as the title dyes, X-ray crystal structures are very valuable in fostering an understanding of the results found by other methods. Despite various attempts, however, single crystals suitable for X-ray structural analysis could only be obtained for **1a** by slow diffusion of hexane into a solution of the compound in dichloromethane. The cell parameters and refinement details for **1a** are summarised in Table S1 in the Supporting Information. Figure 1 shows that the indacene plane of **1a** is almost planar with the average deviation of the ring atoms amounting to 0.0135 Å, which is similar to the classic BODIPY derivatives.[19,29,52–60] The bond lengths and angles of the indacene ring system are also close to the values of previously reported BODIPY compounds. The molecules are packed parallel

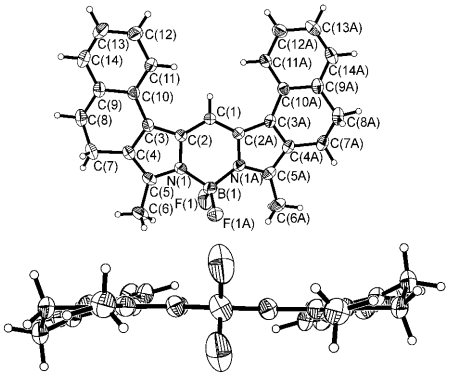

Figure 1. Crystal structure of **1a** with 30% probability thermal ellipsoids (top: perspective view; bottom: side view along the B(1)–C(1) axis). Selected bond lengths [Å] and bond angles [°]: B1–F1 1.367(2), B1–N1 1.543(3), N1–C2 1.383(2), N1–C5 1.360(2), C1–C2 1.381(2), C2–C3 1.425(3), C3–C4 1.379(2), C4–C5 1.394(3); N1-B1-N1A 107.5(3), F1-B1-F1A 109.2(3), C2-C1-C2A 123.3(3).

to each other with alternating tail-to-tail orientation along the crystallographic *a* axis (Figure 2). Therefore, no π–π stacking interactions can be observed. However, it is very interesting to note that the neighbouring BODIPY molecules are linked through intermolecular hydrogen bonds (C–H···F = 2.508 Å) between the BF_2 and H atoms of the dihydronaphthalene ring to form a zigzag chain along the *c* axis (Figure 3).

Absorption and fluorescence spectroscopy: To obtain detailed information on the effect of conformationally locked phenyl substitution at the 1,7-

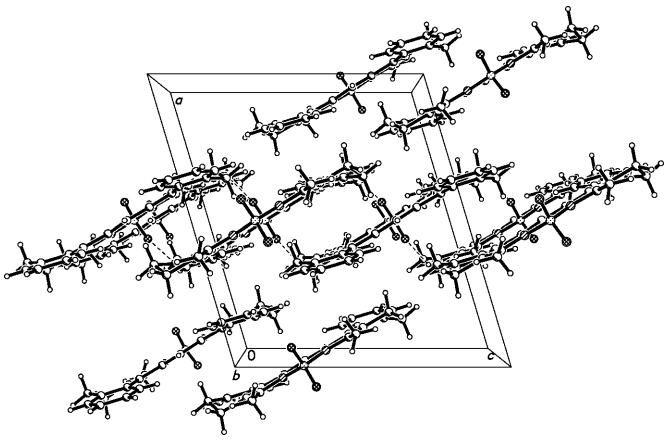

Figure 2. Molecular packing in the crystal structure of **1a** along the *a* axis.

positions on the photophysical characteristics of the title dyes, **1a–d** and **2** have been investigated by absorption as well as steady-state and time-resolved fluorescence spectroscopy in a variety of solvents that span the polarity range from hexane to methanol. The absorption (λ_{abs}) and emission maxima (λ_{em}), bandwidths at half-maximum height (fwhm), Stokes shifts ($\Delta\tilde{\nu}_{abs-em}$), fluorescence quantum yields (Φ_f) and lifetimes (τ_f) along with radiative and nonradiative constants (k_r and k_{nr}) derived from the experimental data are included in Table 1. Figure 4 contains representative absorption and emission spectra for **1a–c** and **2** in dibutyl ether, and for **1d** the corresponding spectra in a series of solvents of different polarity are shown in Figure 5.

***meso*-Carbon derivatives 1a–d**: The absorption maxima of compounds **1a**, **1b** and **1d** are centred at approximately

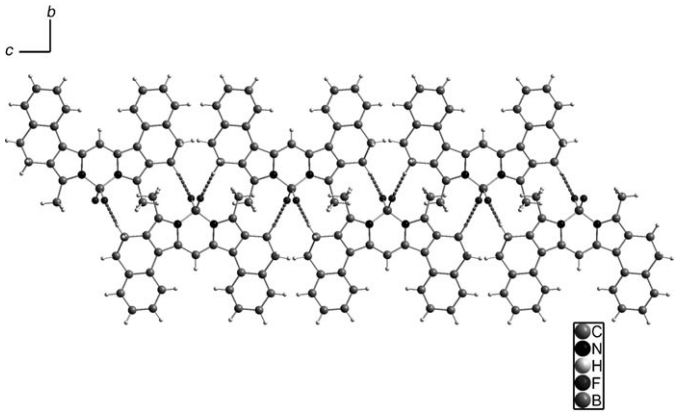

Figure 3. One-dimensional zigzag chain formed through hydrogen bonds along the *c* axis (for a colour version of the figure, see Figure S1 in the Supporting Information).

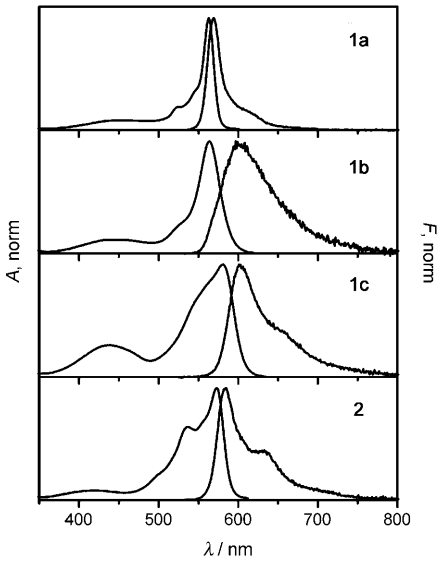

Figure 4. Normalised absorption and fluorescence spectra of **1a–c** and **2** in dibutyl ether at 298 K.

560 nm and are independent of solvent polarity, with only a small variation of 3–4 nm upon going from methanol to

Table 1. Spectroscopic and photophysical properties of **1a–d** and **2** in various solvents at 298 K.

	Solvent	λ_{abs} [nm]	$fwhm_{abs}$ [cm^{-1}]	λ_{em} [nm]	$fwhm_{em}$ [cm^{-1}]	$\Delta\tilde{\nu}_{abs-em}$ [cm^{-1}]	Φ_f	τ_f [ns]	k_r [$10^8\ s^{-1}$]	k_{nr} [$10^8\ s^{-1}$]
1a	MeOH	559	660	566	690	240	0.50	3.36	1.5	1.5
	MeCN	558	720	566	740	270	0.52	3.37	1.5	1.4
	THF	562	630	569	680	220	0.55	3.30	1.7	1.4
	Et_2O	561	560	567	647	240	0.54	3.29	1.6	1.4
	Bu_2O	563	525	568	630	200	0.54	3.24	1.7	1.4
	hexane	562	480	567	590	170	0.54	3.05	1.8	1.5
1b	MeOH	559	1140	598	2220	1240	0.36	2.63	1.4	2.4
	MeCN	559	1280	599	2170	1280	0.38	3.18	1.2	1.9
	THF	562	1070	599	2190	1170	0.44	3.47	1.4	1.4
	Et_2O	561	1100	601	2170	1240	0.44	3.33	1.3	1.7
	Bu_2O	563	1060	601	2170	1210	0.51	3.42	1.5	1.4
	hexane	564	1060	601	2160	1170	0.52	3.56	1.5	1.3
1c	MeOH	569	2090	612	2110	1240	0.11	1.21	0.9	7.4
	MeCN	565	2080	612	2300	1360	0.10	1.30	0.8	6.9
	THF	573	2010	609	1830	1030	0.23	2.24	1.0	3.4
	Et_2O	576	2010	605	1650	840	0.29	2.97	1.0	2.4
	Bu_2O	581	1950	602	1370	640	0.39	3.26	1.2	1.9
	hexane	584	1890	598	1070	470	0.46	3.97	1.2	1.4
1d	MeOH	556	1270	567	1550	450	0.059	0.15 (0.62) 3.32[a]	–	–
	MeCN	554	1120	573	1640	680	0.014	0.11[b]	1.2	90
	THF	558	910	575 (LE) 728 (CT)	350 (LE) 3250 (CT)	560 (LE) 4200 (CT)	0.074	0.01 3.22[c]	–	–
	Et_2O	557	850	572 (LE) 649 (CT)	350 (LE) 3220 (CT)	480 (LE) 2570 (CT)	0.16	0.03 4.13[c]	–	–
	Bu_2O	559	830	571	1150	430	0.36	3.45	1.0	1.9
	hexane	560	870	570	1180	360	0.32	2.72	1.2	2.5
1d-H^+	MeCN	564	1120	585	1640	680	0.38	3.46	1.1	1.8
2	MeOH	558	2725	581	2021	673	0.62	3.12	2.0	1.2
	MeCN	558	2820	582	1970	770	0.66	3.43	1.9	1.0
	THF	566	2370	582	1920	560	0.73	3.43	2.1	0.8
	Et_2O	567	2100	581	1880	445	0.76	3.80	2.0	0.6
	Bu_2O	572	1880	583	1770	390	0.79	3.55	2.2	0.6
	hexane	576	1030	583	1000	230	0.77	3.90	2.0	0.6

[a] Both species are only found in the region of the typical BODIPY-localised emission. Their amplitudes are always positive and the amplitude ratio is constant over the measured emission range of 560–650 nm. The value in brackets represents the relative amplitude of the fast decay component; see text for discussion. [b] A trace of a slow component with 3.23 ns is also found; see text for discussion. [c] The two components show a typical precursor–successor relationship with a positive amplitude ratio r_a in the blue and a negative ratio in the red part of the spectrum. For **1d** in Et_2O and THF, $r_a = a_1/a_2 = -1$ at >650 and >680 nm, respectively (subscripts 1 and 2 denote fast and slow decay components, respectively).

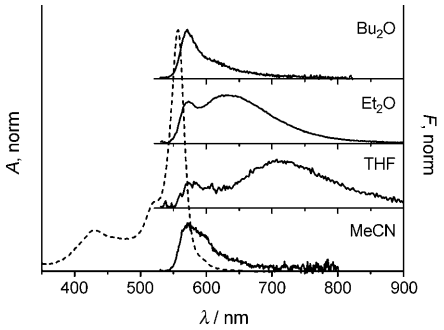

Figure 5. Absorption spectrum of **1d** in diethyl ether (– – –; the absorption spectra in the other solvents are very similar, see Figure 7) and fluorescence spectra (——) of **1d** in dibutyl ether (Bu_2O), diethyl ether (Et_2O), tetrahydrofuran (THF) and acetonitrile (MeCN) at 298 K.

hexane. In the case of **1c**, however, a more pronounced correlation of λ_{abs} with solvent polarity is observed, thereby resulting in a hypsochromic shift of approximately 15 nm when increasing the solvent polarity from hexane to methanol (Table 1). Additionally, the absorption of **1c** in nonpolar solvents is redshifted for approximately 20 nm with respect to that of **1a**, **1b** and **1d**. It is also evident from Figure 4 and Table 1 that the absorption spectra of **1c** are more than twice as broad as those of the other dyes, the full width at half-maximum height ($fwhm_{abs}$) of the spectra of the compounds decreasing in the order of $fwhm_{\mathbf{1c}} \approx 2 \times fwhm_{\mathbf{1b,d}} \approx 4 \times fwhm_{\mathbf{1a}}$. On the other hand, the increase in the width of a spectrum is connected to a reduction in molar absorption coefficient from, for example, $\varepsilon_{562\,nm} = (111\,700 \pm 2240)\,M^{-1}cm^{-1}$ for **1a** to $\varepsilon_{563\,nm} = (76\,800 \pm 1570)\,M^{-1}cm^{-1}$ for **1b** in THF. This suggests that the overall integrals of the longest-wavelength absorption bands do not change too much. However, from a comparison of the fwhm and the shape of the spectra of **1a–d** and **2** with those of entirely planar BODIPYs such as **12a** (Scheme 2), for example, $fwhm_{abs}^{THF}(\mathbf{1a}) = 630\ cm^{-1}$ versus $fwhm_{abs}^{THF}(\mathbf{12a}) = 490\ cm^{-1}$,[29] it is obvious that even the spectra of **1a** are broader and do not show the typical cyanine-type vibronic structure as planar BODIPYs do. The absorption data reported here thus suggest that more than one optical transition is contributing to the intense band in the 500–600 nm region, which is supported by a more detailed theoretical treatment that identifies three transitions (see below).[61]

Recent studies of phenanthrene-appended BODIPYs have shown that for such crowded derivatives, the *meso*-aryl-substituted BODIPY chromophore can adopt a propeller-like geometry, thereby leading to an intramolecular twisting angle between the BODIPY core and the *meso*-aryl group θ_{MP} of significantly less than 90° (i.e., no perpendicular orientation; Figure 6).[30] If a *meso*-substituted BODIPY deviates from the perpendicular structure (Figure 6D), in principle two different conformations are possible, the already mentioned propeller-type (Figure 6A) and a butterfly-type structure (Figure 6B). (The latter butterfly-type structure can potentially also accommodate a perpendicular arrangement of the *meso* group, as shown in Figure 6C.) In

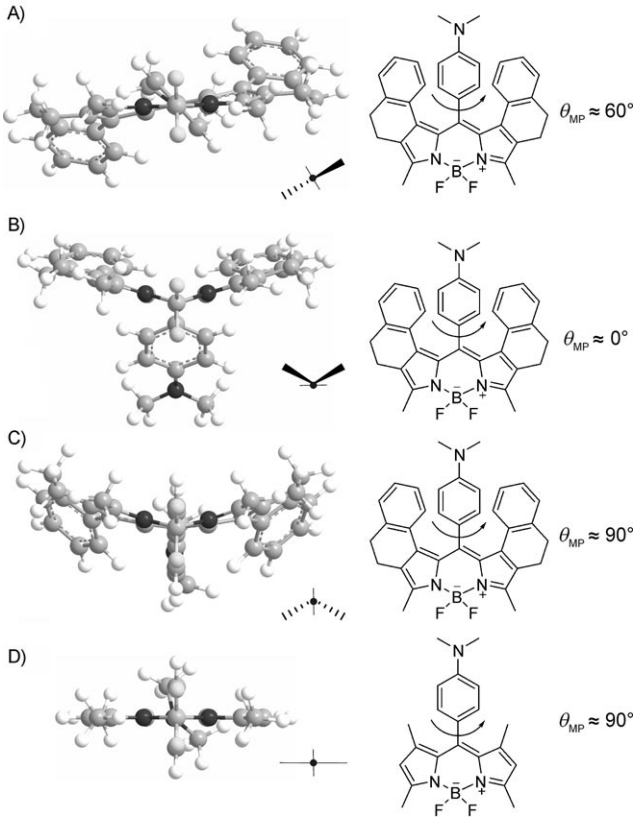

Figure 6. Possible conformations of sterically crowded (A–C) and conventional (D) BODIPYs, viewed along the B–C_{meso} axis. A) Hypothetical propeller-like conformation of **1d**. Hypothetical butterfly-like conformations of **1d** with B) kinked–parallel and C) perpendicular orientation of the *meso* ring. D) Perpendicular conformation of **3a**. The pictograms denote the orientation of the benzo rings of the dihydrobenzo[*e*]isoindole (A–C; or the pyrrole rings in D) and the *meso*-phenyl ring with respect to the central six-membered diazaborinane ring. Solid wedges indicate upward-facing and dashed wedges downward-facing moieties. In D, the two methyl groups of the aniline moiety are out of the vertical plane to some (different) degree; the phenyl ring is perpendicular. The impact of the conformational constraints on the relative energies of the structures shown in A–C can be deduced from the data given in Table 2 and ref. [70]. For a more detailed discussion, see the sections on the theoretical results.

the first case, for $\theta_{MP} \approx 60°$, a certain conjugation between the *meso* group and BODIPY core can arise. As has been shown for a 1,7-hydrogen-substituted *meso*-(4-dimethylamino)phenyl BODIPY derivative (**10b**, with $\theta_{MP} = 48.9°$; Scheme 5), such a predisposition can lead to a charge-transfer (CT) transition already in absorption, for instance, from the anilino group to the BODIPY moiety, which can be traced in the absorption spectra as broad, structureless and solvatochromic bands.[32] Although such bands are not readily obvious from the spectra, we scrutinised the absorption spectra of **1d** more thoroughly by analysis of the first-derivative absorption spectra in hexane, dibutyl ether, diethyl ether, THF and acetonitrile.[62] However, in contrast to **10b**, no contributions of a broad and solvatochromic band were found here for **1d** (Figure 7). The only difference between **1d** and **1a–c** is the appearance of a weak band at wave-

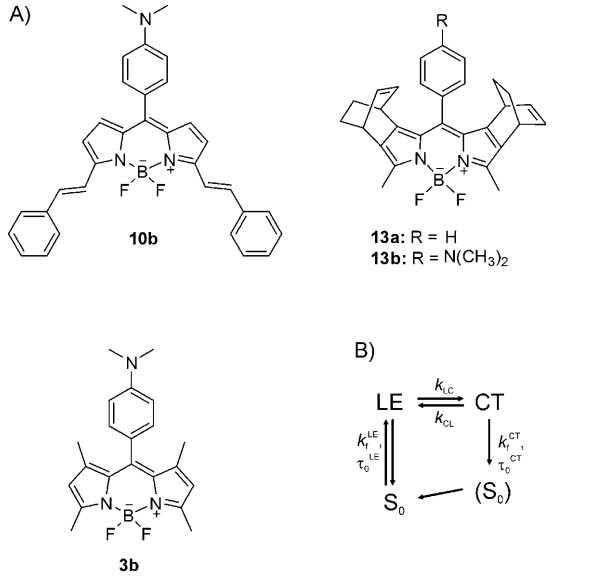

Scheme 5. A) Chemical structures of charge-transfer-active BODIPYs **10b**, **13b** and **3b** (**13a** = parent of **13b**); B) Excited-state precursor–successor reaction mechanism often found in BODIPYs such as **3b**, **13b** and **1d**.

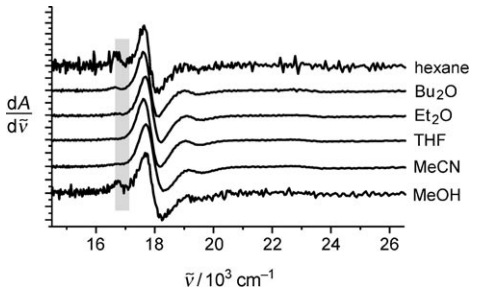

Figure 7. First derivatives of the absorption spectra of **1d** in the solvents indicated in the plot. The grey bar corresponds to the region of the weak band on the low-energy side. The noise on the hexane and methanol spectra is due to the limited solubility of the dye in those two solvents.

lengths >580 nm (equivalent to the grey bar at $<17250\ cm^{-1}$ in Figure 7), which shows only a negligible shift with solvent polarity and is least developed in polar non-protic solvents.

With respect to the emission spectra, the influence of the *meso* substituents is generally more pronounced. Whereas the emission maxima of **1a** and **1d** are found at approximately 570 nm, those of **1b** are centred at approximately 600 nm and those of **1c** at approximately 605 nm, the latter again showing a trend that depends on solvent polarity, now a hypsochromic shift of approximately 15 nm when decreasing solvent polarity from methanol to hexane (Table 1). Distinct differences are also found for $fwhm_{em}$: the order now is $fwhm_{\mathbf{1b}} \approx 2 \times fwhm_{\mathbf{1d}} \approx 4 \times fwhm_{\mathbf{1a}}$. For **1c**, $fwhm_{em}$ decreases twofold upon going from polar to non-polar solvents (Table 1). Accordingly, the aforementioned results yield the following trends for the Stokes shifts. Compound **1a** shows the most resonant bands with $\Delta\tilde{\nu}_{abs-em} \approx 210\ cm^{-1}$, followed by **1d** with approximately $500\ cm^{-1}$ and **1b** with $1200\ cm^{-1}$. Because of the opposite solvatochromic shifts in both absorption and emission, the Stokes shift of **1c** increases from approximately $500\ cm^{-1}$ in hexane to approximately $1350\ cm^{-1}$ in acetonitrile. However, the position of the 0,0-transition of **1c** remains virtually unchanged when taking $E_{00} = (E_{abs} - E_{em})/2$ as a measure, for example, $E_{00}^{Hex} = 16930\ cm^{-1}$ and $E_{00}^{MeOH} = 16980\ cm^{-1}$, or, more globally, $E_{00}^{solvents} = (16967 \pm 34)\ cm^{-1}$ with superscript "solvents" referring to all solvents included in Table 1.[63] Concerning **1d**, the fluorescence data described so far relate only to the weakly Stokes-shifted, narrow emission of typical BODIPY-type shapes. In solvents more polar than dibutyl ether, however, a second, broad and largely redshifted emission band is found, its maximum showing strong solvatochromism (Figure 5, Table 1).

The fluorescence quantum yields are considerably high and independent of solvent polarity for **1a** (0.53 ± 0.03) and decrease 1.5- and 4-fold upon going from less (hexane) to more (methanol) polar solvents for **1b** and **1c** (Table 1). For **1a–c**, these trends are reflected by the fluorescence lifetimes, which are mono-exponential in all cases (Table 1). Accordingly, the rate constants of radiative deactivation are constant and virtually identical for **1a**,**b** ($k_r = (1.5 \pm 0.3) \times 10^8\ s^{-1}$) and slightly lower for **1c** ($k_r \approx 1.0 \times 10^8\ s^{-1}$).[64] The rate constants of non-radiative deactivation amount to $k_{nr} = (1.5 \pm 0.2) \times 10^8\ s^{-1}$ for **1a** and **1b** in non-polar solvents and are slightly increased for **1b** in MeCN and MeOH. Compound **1c** shows a similar $k_{nr} = 1.4 \times 10^8\ s^{-1}$ in hexane and a progressive increase to $k_{nr} = 7.4 \times 10^8\ s^{-1}$ in methanol. For **1d** in the absence of CT emission, k_r and k_{nr} are virtually identical to those of **1c**. These results suggest that for all the dyes (i.e., for **1d** in non-polar solvents only), the nature of the emitting state does not change upon altering solvent polarity. However, the partly strong variation of $fwhm_{em}$ suggests that the conformational diversity can be considerably influenced by solute–solvent interactions.

Since no hints for a CT absorption band were found in the region of 510–530 nm (see discussion above), excitation of **1d** at 520 nm should lead to exclusive excitation of a BODIPY core-centred transition. In the medium and polar solvents, the *CT state can thus only be populated from the (relaxed) Franck–Condon excited state in a typical precursor–successor excited-state reaction (Scheme 5). Analysis of the dual fluorescence of **1d** in diethyl ether and THF is thus possible with the respective procedure for such a reaction mechanism and leads to the following photophysical parameters (for a detailed description of the procedure, see ref. [65]). The ratio of charge-transfer to BODIPY-localised (or locally excited (LE)) fluorescence amounts to $\Phi_f(CT)/\Phi_f(LE) = 3.9$ and 6.7, respectively. These values are of the same order of magnitude as those found for **3b** (Scheme 5) with $\Phi_f(CT)/\Phi_f(LE) = 4.2$ and 9.0 in Et_2O and THF,[65] respectively, but distinctly higher than $\Phi_f(CT)/\Phi_f(LE) = 0.2$ of a sterically more hindered BODIPY derivative, **13b**, in THF.[29] These findings suggest that the efficiency of CT state formation in **1d** is higher than in **13b**, most likely be-

cause of the different conformations of the sterically crowded **1d** ($\theta_{MP}=54.9°$ as obtained from geometry optimisation in the gas phase, see below) and **13b** ($\theta_{MP}=65°$ for parent **13a** by X-ray structure analysis).[29] Following the procedure in ref. [65], the excited-state reaction dynamics of **1d** in, for instance, Et_2O are determined to be $k_{LC}=17.9\ ps^{-1}$, $k_{CL}=13.1\ ps^{-1}$, and $(\tau_0^{CT})^{-1}=0.21\ ps^{-1}$ (for parameters, see Scheme 5). The ratio of the excited-state reaction rate constants $k_{LC}/k_{CL}=1.4$ suggests that CT state population (the forward excited-state reaction) is efficient, yet the backward excited-state reaction is not negligible in such less twisted but sterically constrained derivatives. The sterically demanding but more rigid bicyclo moieties in **13b** seem to aggravate the backward reaction ($k_{LC}/k_{CL}=8.9$)[29] and, finally, the back reaction is even less efficient in **3b** with $k_{LC}/k_{CL}=18$ in diethyl ether.[65] In acetonitrile and methanol, however, the CT emission band could not be observed here for **1d**, most likely because of the small energy gap and efficient internal conversion in these highly polar solvents. In acetonitrile, only the traces of a slow decay component in the region of LE emission hint at CT state formation (Table 1). On the other hand, the threefold increase of fluorescence upon going from a highly polar non-protic (MeCN) to a highly polar protic solvent (MeOH) also supports the assignment of a CT process to the quenching process. Solute–solvent interactions between solvent molecules and the nitrogen atom of the *meso*-anilino group through hydrogen bonding lead to a certain reduction of the CT driving force. This is also supported by the fluorescence lifetime data in Table 1 (i.e., a larger amplitude of a slow decay component in the LE region in methanol, most likely arising from hydrogen-bonded species). Accordingly, protonation also blocks the CT process (see below).

An analysis of the fluorescence anisotropy (r) data of **1a–c** in glycerol at 278 K provided further information on the orientation of absorption and emission dipoles within the title molecules (Figure 8). Values of r close to 0.4 are found in the region of the BODIPY bands (i.e., above 500 nm).[66] The dipoles of the transitions responsible for the absorption and emission processes are thus highly co-linear and oriented along the cyanine-type BODIPY π system.[67]

The experimental data discussed so far suggest that an increase in bulkiness of R_{meso} leads to a broadening of the spectra, a certain loss of emissivity and an increase of the influence of the nature of the solvent, with the step from $R_{meso}=$ methyl (**1b**) to $R_{meso}=$ phenyl (**1c**) being more dramatic. The findings further indicate that the diversity of ground-state conformations is much higher in **1c** than in **1b** and especially **1a**. The behaviour of **1c** further indicates that interactions with the solvent play a certain role, that is, polar solvents facilitate conformational diversity.

***meso*-Nitrogen derivative 2**: According to Table 1 and Figure 4, the spectroscopic properties of **2** are rather similar to those of the **1** series. The absorption maxima are centred at approximately 565 nm and show a hypsochromic shift of approximately 20 nm when increasing solvent polarity from hexane to MeCN/MeOH. Whereas the emission maxima, centred at (582 ± 1) nm, are not affected by solvent polarity, both the widths of absorption and emission bands increase with an increase in the solvent polarity. Consequently, the Stokes shifts increase from 230 cm^{-1} in hexane to 770 cm^{-1} in acetonitrile. The fluorescence quantum yields are high and show a slight positive solvatokinetic behaviour (i.e., are slightly reduced from 0.77 in hexane to 0.62 in methanol). The fluorescence lifetimes correspond to the quantum-yield data, thus leading to virtually constant $k_r=(2.1\pm0.2)\times10^8\ s^{-1}$ and k_{nr} that slightly increase toward polar solvents. However, when the fact that the width of the fluorescence bands increases in polar solvents is taken into account by excluding the dependence of k_r on the emission spectrum and considering the reduced rate constants κ_f,[64] virtually no influence is found: $\kappa_f=(1.6\pm0.1)\times10^5\ s^{-1}cm^3$ regardless of solvent polarity. The molar-absorption coefficient $\varepsilon_{566\,nm}=(58\,130\pm750)\ M^{-1}cm^{-1}$ is lower than that of **1a** (see above), but, considering the different $fwhm_{abs}$, integrals of similar magnitude are found for the bands in the 500–600 nm region. The fluorescence anisotropy data shown in Figure 8 also indicate co-linear absorption and emission dipoles.

The most striking finding of the present investigation is the similarity of the spectroscopic properties of **1a–c** on one

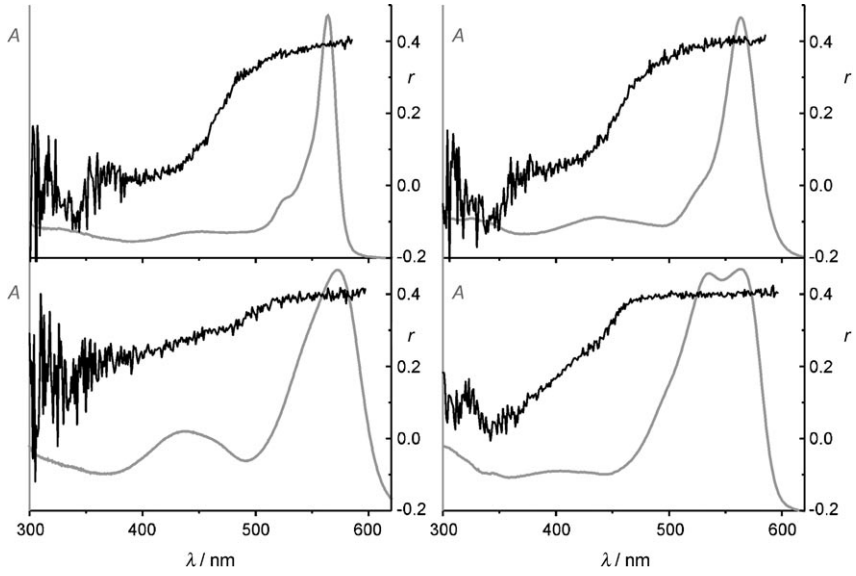

Figure 8. Fluorescence anisotropy r (black) of **1a** (top, left), **1b** (top, right), **1c** (bottom left) and **2** (bottom right) measured in glycerol at 278 K. The absorption spectra in the same solvent at 298 K are plotted in grey.

and **2** on the other side. The absorption features of **2** compare well with those of **1c** and the emission features resemble an intermediate of those of **1a**,**b**. These findings are in striking contrast to the modulations observed so far for *meso*-atom exchange in BODIPYs, that is, bathochromic shifts of approximately 100 nm and distinctly lower fluorescence quantum yields as mentioned in the Introduction; see Scheme 2 (e.g., **6** vs. **7** or **8** vs. **9**) and the discussion in the text above.

Quantum chemical calculations: To better understand the findings of the spectroscopic measurements and to elucidate the differences within the series of title dyes and with respect to related dyes of the literature in a more detailed manner, density functional theory (DFT) as well as time-dependent DFT (TD-DFT) calculations were performed with the B3LYP functional and the 6-31G(d) basis set as implemented in Gaussian 03.[68,69] In all cases, two different starting geometries were employed, a "propeller-like" and a "butterfly-like" one (Figure 9), which all converged.[70]

Optimised geometries: From Table 2 it is obvious that for all compounds except for **1b**, the propeller-like (P) optimised structure is more stable than the butterfly-like (B) structure. The adoption of a P conformation in the case of **1a** is confirmed experimentally by the X-ray structure (Figure 1 and Figure S2 in the Supporting Information). For **1b**, however, the B conformation seems to be more favoured. Taking the dihedral angle between the two pyrrole rings (θ_{PP}) as a measure for the co-planarity of the indacene core (Table 2), it is evident that in all cases the P structure is the more co-planar one except, again, for **1b**.

On one hand, co-planarity of the indacene core is an important prerequisite for strong electronic conjugation in the chromophore and, together with good molecular orbital (MO) overlap, guarantees often favourable fluorescence features and high oscillator strengths. On the other hand, the adoption of a B or P conformation is also important for the degree of coupling or decoupling between BODIPY core and *meso* substituent. Especially for **1d** with a *meso*-dimethylanilino substituent, a less decoupled structure has to be considered in the context of a possible intramolecular charge-transfer process. Figure 9 shows that the twisting angle around the C_{meso}–C_{phenyl} bond θ_{MP} is distinctly different for both structures, that is, close to a perpendicular arrangement ($\theta_{MP}=86.7°$) in **1d**(B) but less twisted ($\theta_{MP}=59.8°$) for **1d**(P). The influence of the electronic nature of the group in the *meso* position should thus be higher in the case of P conformations.[71]

The structural features as derived from the DFT calculations yield dihedral angles between the two pyrrole rings of the indacene core $\theta_{PP}=5.9$, 19.0, 20.0 and 1.4° for the more stable P conformation of **1a**, **1c**, **1d** and **2** and 7.8° for **1b**(B), respectively. Since the alignment of the transition dipoles is virtually identical for the dyes, the degree of planarity of the molecular structures presumably accounts for the order of calculated oscillator strengths *f* (Table 3 and Figure S4 in the Supporting Information) and experimentally derived Φ_f (or k_r or κ_f, Table 1 and Table S2) values (i.e.,

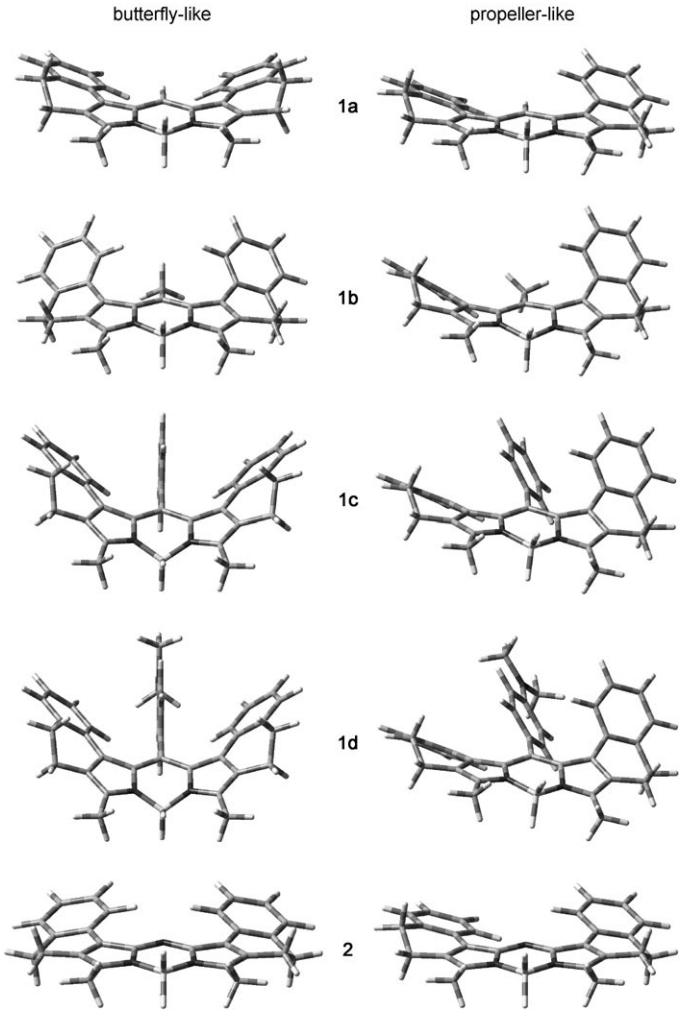

Figure 9. Optimised ground-state geometries of compounds **1a–d** and **2** obtained from DFT calculations with the B3LYP functional and the 6-31G(d) basis set. The converged structures for a "butterfly-like" starting geometry are shown on the left and those for a "propeller-like" starting geometry on the right. For a comparison of the calculated structures of **1a** with the X-ray structure, see Figure S2 in the Supporting Information.

Table 2. Results of the geometry optimisations of the ground state (B = "butterfly-like" conformation, P = "propeller-like" conformation); for self-consistent field (SCF) energies, see Table S4 in the Supporting Information.

	Structure[a]	ΔE[b] [kJ mol^{-1}]	μ_g[c] [D] B	μ_g[c] [D] P	θ_{PP}[d] [°] B	θ_{PP}[d] [°] P
1a	P	0.8	2.9	3.0	6.0	5.9
1b	B	9.4	3.2	4.3	7.8	19.6
1c	P	25.8	3.9	3.7	27.5	19.0
1d	P	29.7	6.1	6.9	26.8	20.0
2	P	2.5	1.7	1.7	2.0	1.4

[a] Structure of the most stable conformation. [b] Energetic gain of the most stable with respect to the other ("butterfly-" or "propeller-like") conformation. [c] Ground state dipole moment. [d] Dihedral angle between the two planes defined by the five atoms of the two pyrrole rings.

Table 3. Calculated properties for the vertical excitation of the most stable energy-minimised ground-state geometries of the title dyes and model compounds **5b**, **6**, **7** and **10b** by TD-DFT (for calculation details, see the Experimental Section).

	$\lambda_{S_n \leftarrow S_0}(n)$[a] [nm]	f[b]	$\Delta\mu_{S_n-S_0}$[c] [D]	Orbitals (coefficients)[d]
1a(P)	472.1 (1)	0.482	3.9	HOMO–LUMO (0.438)
				HOMO−1–LUMO (0.468)
	456.3 (2)	0.297	−2.9	HOMO–LUMO (−0.400)
				HOMO−1–LUMO (0.478)
	438.0 (3)	0.115	3.3	HOMO−2–LUMO (0.668)
1b(B)	472.8 (1)	0.668	1.7	HOMO–LUMO (0.526)
				HOMO−1–LUMO (−0.333)
	463.3 (2)	0.087	−1.7	HOMO–LUMO (0.284)
				HOMO−1–LUMO (0.582)
	437.6 (3)	0.094	2.7	HOMO−2–LUMO (0.669)
1c(P)	484.7 (1)	0.316	3.4	HOMO–LUMO (0.359)
				HOMO−1–LUMO (0.552)
	466.4 (2)	0.385	−3.6	HOMO–LUMO (0.478)
				HOMO−1–LUMO (−0.384)
	462.6 (3)	0.042	3.8	HOMO−2–LUMO (0.673)
1d(P)	521.3 (1)	0.053	16.0	HOMO−1–LUMO (0.676)
	478.0 (2)	0.422	2.5	HOMO–LUMO (0.443)
				HOMO−2–LUMO (0.472)
	462.4 (3)	0.245	−3.7	HOMO–LUMO (−0.409)
				HOMO−2–LUMO (0.480)
	434.9 (4)	0.153	4.6	HOMO−3–LUMO (0.665)
2(P)	545.4 (1)	0.181	4.8	HOMO–LUMO (−0.314)
				HOMO−1–LUMO (0.576)
	498.1 (2)	0.124	3.7	HOMO−2–LUMO (0.661)
	492.8 (3)	0.532	−1.2	HOMO–LUMO (0.477)
				HOMO−1–LUMO (0.325)
5b	517.5 (1)	0.708	−2.3	HOMO–LUMO (0.593)
6	495.0 (1)	0.760	−3.2	HOMO–LUMO (0.602)
7	561.2 (1)	0.719	−0.4	HOMO–LUMO (0.571)
10b	558.0 (1)	0.876	−4.1	HOMO–LUMO (0.596)
	508.4 (2)	0.516	20.2	HOMO−1–LUMO (0.666)

[a] Wavelength of the transition. The next highest transitions of **1a–d**, **2** and **5b** are found at <400 nm; see Figure S5 in the Supporting Information. [b] Oscillator strength of the transition. [c] Dipole moment difference between ground (μ_0) and respective excited (μ_n) state. [d] MOs involved in the transitions.

1a>**1b**>**1c**). Moreover, because the probability of intersystem crossing is very low in BODIPY dyes,[72] k_{nr} can be mainly attributed to internal conversion processes, which are related to the flexibility/rigidity of the dye.[73] The increased k_{nr} of **1c** and **1d** in non-polar solvents thus seem to be a direct consequence of the structural features. The dipole moments calculated for **1a**(P), **1b**(B) and **1c**(P) are rather similar and not very pronounced with $\mu_g \approx 3.5$ D, those of **1d**(P)/**2**(P) are somewhat higher/lower (Table 2).

Molecular orbitals and transitions: Figures 10 and 11 show the frontier molecular orbitals of **1a–d** and **2** as well as those of the model compounds **5b**, **6**, **7** and **10b** (Schemes 2 and 5). Table 3 collects the relevant lowest-energy transitions. As can be deduced from Figure 10, for the title dyes, HOMO and LUMO are almost identically localised, mainly on the BODIPY core and less on the dihydronaphthalene (DHN) fragments. Only HOMO−1 and HOMO−2 (or, in the case of **1d**, HOMO−2 and HOMO−3) are rather evenly localised on the entire DHN-BODIPY chromophore, whereas LUMO+1 is predominantly localised on the DHN fragments. For **1a**,**b** and **2**, the *meso* atom and the appended R_{meso} do not participate in any of the occupied orbitals shown as well as LUMO+1. In addition to the *meso* atom, carbon atoms 1 and 7 (see Scheme 1 for numbering) also do not participate significantly in the HOMO−1 and HOMO−2 in **1a–c** or HOMO−2 and HOMO−3 in **1d**. However, in accordance with general BODIPY photophysics, a high coefficient is found on the *meso* atom and C1 and C7 in the LUMO. In the case of **1c**,**d**, the *meso* group participates in the HOMO−2/HOMO−3 and the LUMO+1; only for **1d**, HOMO−1 shows high orbital coefficients on the *meso* group. According to Table 3, the two lowest transitions are mixed HOMO–LUMO and HOMO−1–LUMO transitions for **1a–c**; $S_3 \leftarrow S_0$ is then a HOMO−2–LUMO transition. It is also apparent that the three lowest transitions are rather close-lying in energy/wavelength. The calculated oscillator strengths for the $S_1 \leftarrow S_0$ and $S_2 \leftarrow S_0$ transitions in the dyes with a more stable P conformation are considerably high, and they increase with a larger contribution of the HOMO–LUMO transition. Although the absolute positions of the calculated transitions in the gas phase show a hypsochromic displacement for all the dyes studied here, their sequence agrees rather well with the measured absorption spectra in solution (Figure S5 in the Supporting Information; some exceptions for **1d** and **2** are discussed below). This agreement stresses the phenomenological interpretation made above that, in contrast to **3** or **12**, the single-transition, cyanine-type absorption features of the lowest-energy absorption bands of those planar BODIPY dyes are not found here or are at least superimposed by other transitions. If we assume that the three lowest transitions contribute to the absorption band in the 500–600 nm region, a comparison of the sum of their oscillator strengths Σf_i (with $i=1, 2, 3$) with θ_{PP} yields the expected trend within the series **1a–c**, that is, Σf_i is the larger the smaller the inter-plane angle (Figure S4 in the Supporting Information).

If the solvent is taken into account in the calculations by way of the polarisable continuum model (PCM),[74] that is, as a continuum basically described by the PCM parameters dielectric constant and volume of the solvent molecules, a better agreement of theoretical and experimental absorption maxima is obtained (cf. bathochromic shift between black and coloured bands in Figure S5 in the Supporting Information). Moreover, at least in the case of **1a–c**, theory correctly predicts the slight hypsochromic shift and broadening of the spectra upon going from a hydrocarbon solvent to acetonitrile. The weak solvatochromism is also supported by the theoretical results in which rather small dipole moment changes of opposite signs are found for the three lowest transitions in **1a–c**, thus contributing to the intense band in the visible range.

Position of dihydronaphthalene substitution: To understand why the introduction of aryl substituents in the 3,5-positions

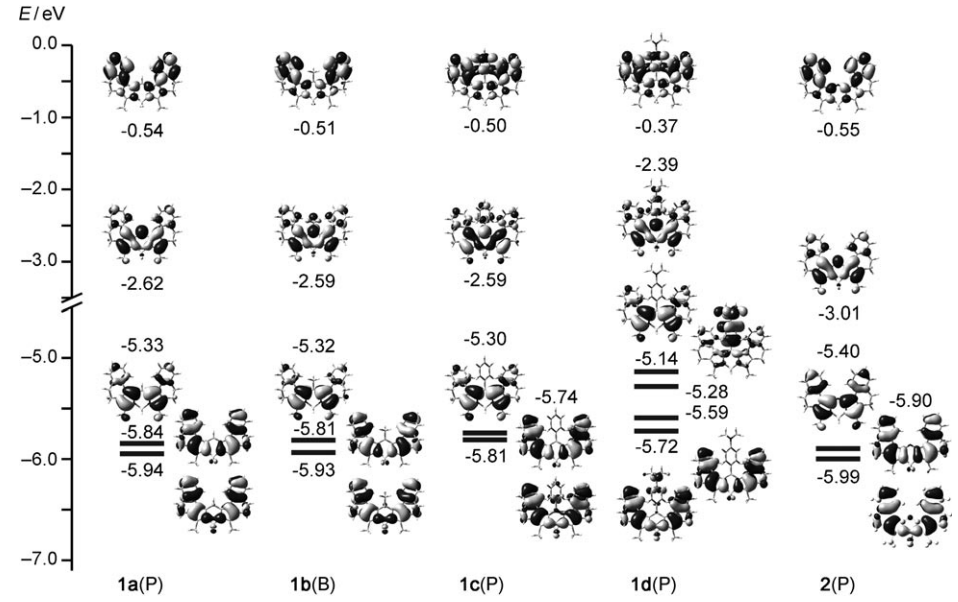

Figure 10. Frontier molecular orbitals of the most stable conformations of the title compounds **1a–d** and **2** (for calculation details, see text).

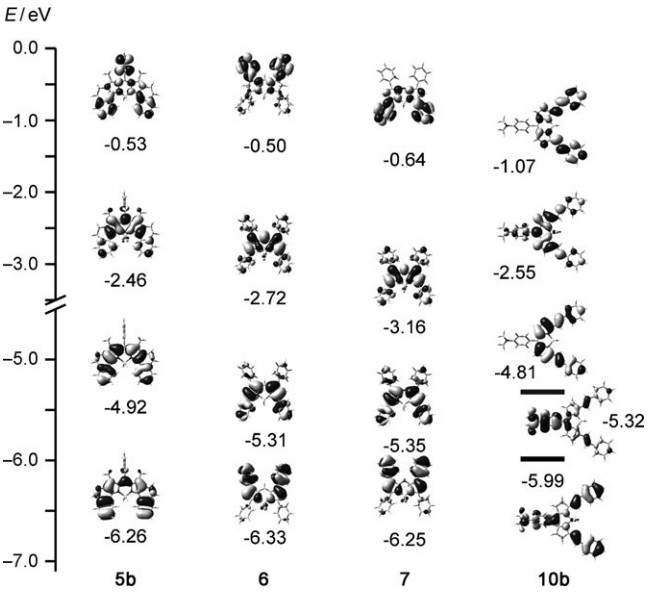

Figure 11. Frontier molecular orbitals of the most stable conformations of the model compounds **5b**, **6**, **7** and **10b** (for calculation details, see text).

of the indacene core is more effective in generating bathochromic shifts, an analysis of the molecular orbitals and transitions obtained by similar calculations for model compound **5b** was carried out as well. The studies revealed that the $S_1 \leftarrow S_0$ transition shows typical cyanine features (i.e., is an oscillator-strong, exclusive HOMO–LUMO transition; Table 3), with the next-highest transition being centred only at 395 nm. For **5b**, HOMO and LUMO are delocalised along the longest polymethinic chain in the entire molecule, the DHN-BODIPY-DHN skeleton, with alternating patterns and large orbital overlap (Figure 11). Again, the electronic density increases in the *meso* position upon electronic excitation. The reduced orbital overlap and the fact that the 1,7-DHN substitution in **1a–c** seems to stabilise the HOMO much better than the 3,5-DHN substitution in **5b** ($\Delta E^{HOMO}_{1a-5b} = -0.41$ eV vs. $\Delta E^{LUMO}_{1a-5b} = -0.16$ eV) are most likely responsible for the less pronounced bathochromic shift when comparing the spectral band positions of **1a–c** and **5b** with **3a**. A similar effect can be observed in model compound **6** (Figure 11), for which all the 1,3,5,7-positions of the BODIPY core are substituted with aryl groups. The contributions of the 1,7-DHN substituents to the HOMO are rather small, and introduction of the DHN groups at these positions again stabilises better the HOMO ($\Delta E^{HOMO}_{6-5b} = -0.39$ eV vs. $\Delta E^{LUMO}_{6-5b} = -0.26$ eV).[75]

Exchange of the *meso* atom: Traditionally, the exchange of the *meso* atom is a means to shift the spectra bathochromically (e.g., from **6** to **7**; Scheme 2). Why this effect is less pronounced in the title dye series when going from **1a** to **2** can be explained in a similar fashion on the basis of the results listed in Table 3 and Figures 10 and 11. Whereas the introduction of the more electronegative atom at the *meso* position leads to a strong stabilisation of the LUMO in **7** with respect to **6** ($\Delta E^{LUMO}_{7-6} = -0.44$ eV vs. $\Delta E^{HOMO}_{7-6} = -0.04$ eV), the effect is less pronounced in **2** compared with **1a** ($\Delta E^{LUMO}_{2-1a} = -0.39$ eV). The concomitant stronger stabilisation of the HOMO ($\Delta E^{HOMO}_{2-1a} = -0.07$ eV) leads to a net decrease in the HOMO–LUMO energy gap difference of $\Delta\Delta E_{1a-2} = 0.32$ eV compared with $\Delta\Delta E_{6-7} = 0.40$ eV. Hence, the bathochromic displacement upon C_{meso} for N_{meso} exchange is larger for the 3,5-DHN-substituted derivatives. In general, however, it has to be emphasised that the TD-DFT calculations at the level of theory employed here are less successful in reproducing the spectroscopic features of **2** than **1a–c** (see the data in Table 1 and Table 3 and the spectra in Figure 4 and S5 in the Supporting Information), despite the fact that the DFT-optimised ground-state geometry seems as realistic as that of **1a–c**. Although the reasons for the higher mismatch are not clear at present, the results described in the next section suggest that specific solute–solvent interactions most likely involving the nitrogen atom at the *meso* position play a certain role.

Charge transfer in 1d and 10b: Closely related to what was discussed in the last paragraph, molecular architecture-based differences in charge-transfer behaviour of *meso*-donor-substituted BODIPYs are an important aspect in the design of BODIPY-derived signalling systems. Here, however, only the entries for the position and the oscillator strength of the transitions of **1d**(P) in Table 3 seem to match with the behaviour of the dye in non-polar solvents. The calculated change in dipole moment (Table 3) and the effects of the solvent in the PCM calculations (Figure S5 in the Supporting Information) do not correspond to the experimentally found trend, that is, a negligible influence of solvent polarity on the absorption spectrum of **1d** (Figure 7). The calculated, pronounced bathochromic shift of the lowest-energy transition from 544 nm in heptane to 589 nm in acetonitrile (Figure S5) is not found in the experiment (Figure 7), but the weak band at >580 nm is even further reduced in THF and MeCN (Figure 7). Apparently, the simplification of exerting the TD-DFT PCM calculations on the gas-phase-optimised S_0 geometry does not account for specific solvation effects, presumably involving the aniline group, that supposedly feed back into the structure. The experimental findings suggest that an increase in solvent polarity facilitates conformational reorganisations in the ground state that lead to a stronger decoupling of the two moieties. Such a decoupling would result in a reduced oscillator strength and an increasingly forbidden character of the lowest-energy (CT) transition; direct population of the highly polarised CT would be aggravated and result in vanishing CT absorption bands and features as shown in Scheme 5B. However, the distinct differences between the prominence of the CT bands in the absorption spectra of **1d** and **10b** are again supported by the calculations: the corresponding $S_2 \leftarrow S_0$ transition in **10b** has a tenfold higher oscillator strength than the $S_1 \leftarrow S_0$ transition in **1d** and is accompanied by a more pronounced dipole moment change, thereby stressing the solvatochromic shift of the CT band in **10b**. When considering that both the localisation of HOMO-1 and LUMO on the molecular fragments and θ_{MP} (54.9 and 48.9°) are comparable for **1d** and **10b**, we tentatively assume that the pronounced difference in the planarity of the extended indacene chromophore is responsible for the different features observed; $\theta_{PP}=20°$ for **1d**(P), yet only 5.7° for **10b**. In addition, the extended chromophore is much more planar in **10b**. Whereas the average twisting angle between the planes of the pyrrole ring and the phenyl ring of the styryl extension θ_E amounts to only 6.1° in **10b**, $\theta_E=29.7°$ for the angle between pyrrole ring and phenyl ring planes of the DHN group in **1d** (see Figure S6 in the Supporting Information for definition of planes).

Photostability of 1a,b and 2: Besides spectroscopic properties, photostability is an important characteristic of a functional dye. Photostability studies were carried out here with **1a**,**b** and **2** in ethanol and compared with rhodamine 101 (Rh101) under identical conditions. Rh101 is usually considered as a benchmark in this wavelength region. The samples were irradiated with a xenon lamp at 560 nm (15 nm slits) with a constant power of 1.7 mW for 8 h. The absorbance of all the samples was adjusted to 0.11 at 560 nm, and the solutions were irradiated in 10×10 mm quartz cuvettes. The investigations revealed that **1a** performed equally well as Rh101, with a decrease of approximately 1–2% (uncertainty ±1%) after 8 h (Figure 12). Compound **1b** showed a slight

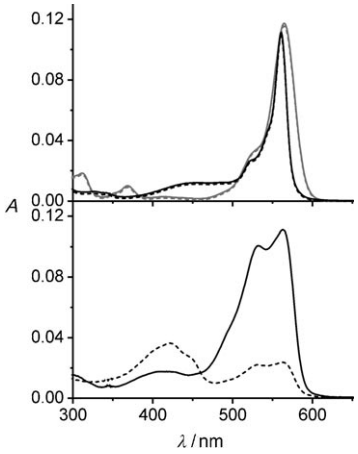

Figure 12. Absorption of **1a** (black) and Rh101 (grey, top) and **2** (bottom) in EtOH before (solid line) and after 8 h of irradiation with an Xe lamp (dashed line). Absorbances for all samples were adjusted to approximately 0.11 at 560 nm before irradiation.

decrease of the absorption band (i.e., a reduction by approximately 5%). In none of the cases was the spectrum modified significantly. However, for **2**, the absorption band at 562 nm showed a significant decrease of 73% after 8 h of irradiation, along with substantial changes of the absorption spectrum; the decrease of the band at 562 nm is accompanied by an increase of a band at 420 nm (Figure 12). The latter indicates the formation of decomposition products, the nature of which, however, could not be clarified during the present studies.

pH-Dependent absorption and fluorescence spectroscopy of 1d: As outlined in the Introduction, the *meso* position is in many cases the position of choice for the integration of an analyte- or a stimuli-responsive group, and since the late 1990s[65,76] many such BODIPY dyes have been developed.[4] However, as we have seen in the previous sections, the degree of twisting around the interannular C_{meso}–C_{phenyl} bond, the degree of conformational confinement and the conjugation in the BODIPY core are decisive parameters for the spectroscopic manifestation of the interaction of the fragments. Hence, the electronic properties of the responsive group themselves also depend on these parameters. Thus, to evaluate the influence of these structural features on the responsiveness of the group in the *meso* position, pH titration experiments were carried out for **1d** and other *meso*-anilino-substituted BODIPYs that we have studied over the past decade in ethanol/water mixtures. Besides **1d**,

this series includes **3b**,[65] **10b**,[32] **12b**,[29] **13b**,[29] **14**,[30] the yet unpublished derivatives **15** and **16**[77] and the three crowned dyes **3c**,[65] **3d**[45] and **3e**[78] (Schemes 5 and 6). At neutral

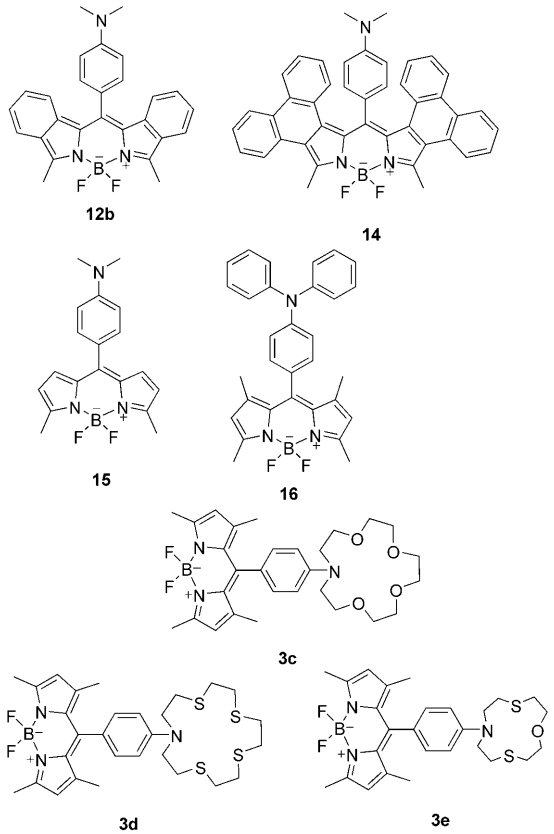

Scheme 6. Chemical structures of selected *meso*-anilino-substituted BODIPYs studied as a function of pH.

pH, all the anilino-substituted derivatives show a strongly quenched fluorescence in the aqueous solvent mixture that was employed, which can be ascribed to the CT quenching process described above for **1d** in more detail. Accordingly, for all the dyes (except **16**; see below), the addition of protons leads to a revival of fluorescence at acidic pH. Protonation at the aniline-N atom suppresses the quenching process and allows the monitoring of the titration curve by fluorometry.[79] Table 4 collects the respective experimental pK_a data and the theoretically obtained twist angles around the C_{meso}–C_{phenyl} bond obtained from the geometry optimised ground-state structures (for computational details, see above and the Experimental Section).

The data in Table 4 allow the derivation of the following rules. Orthogonal decoupling of the dimethylaniline moiety like in **3b** and **12b** yields dyes with pK_a values in between those of non-substituted *N*,*N*-dimethylaniline (DMA: pK_a = 5.07)[80] and DMAs that carry a strongly electron-withdrawing group in the *para* position (4-nitro-DMA: pK_a = 0.65;[80] 4-cyano-DMA: pK_a = 0.18).[81] The reduction of the twisting angle θ_{MP} between the two moieties of the dyes, when considered as DMA–BODIPY dyads, leads to a stronger electronic influence of the electron-deficient BODIPY core and a reduction of the pK_a. The effects of increased steric crowding that forces a dye into the propeller arrangement (like in **1d**, **13b** or **14**) and reduced steric demand that permits a dyad to adopt a more planar conformation (like in **10b** or **15**) are rather similar and suggest that the angle itself is the decisive factor. The result is a linear correlation of pK_a and θ_{MP} (Figure S7 in the Supporting Information). By reconsidering the discussion of the impact of the different P and B conformations on θ_{MP} of **1d** in the theoretical section on optimised geometries above, the protonation studies clearly support the DFT results (i.e., that the most favoured conformation of **1d** is P). When the nature of the substituents on the aniline-N is changed, pronounced differences can arise. For instance, exchange of the methyl groups by phenyl groups leads to a strong delocalisation of the lone electron pair of the nitrogen atom and hampers protonation significantly. On the other hand, introduction of an oxa-crown ether like in **3c** aggravates protonation only slightly, presumably because steric effects and hydrogen-bonding interaction between N^+H and the O atoms of the crown balance each other out. Taking the step from **3c** to **3d** alters the local neighbourhood significantly and the fact that the S atoms show a reduced inductive effect,[82] require more space and cannot stabilise the proton by hydrogen bonding lead to a reduction of the pK_a by >1.5 units. These findings are supported by earlier studies of ours on anilinopyridine dyes for which only the change of the sequence of sulphur and oxygen atoms in crown receptors of identical size led to distinct shifts in the pK_a.[83] A peculiar and at present not fully understood finding concerns the pK_a of crowned **3e**. On the basis of the previous rationalisations, one would expect that the smaller, that is, more crowded ring of the [12]crown-4 receptor along with the presence of two sulphur atoms should lead to an even lower pK_a. However, the opposite is found.[84] Nonetheless, with respect to the DMA derivatives, the present investigations revealed that fine tuning of the pH response is possible by adjusting the interannular twisting angle. As observed for most of the dyes studied earlier, protonation also leads to a strong switching on of the fluorescence of **1d** (Figure 13). The spectroscopic properties of **1d**-H^+ are listed in Table 1.

Table 4. Experimentally determind pK_a values (±0.02) and theoretically obtained twist angles θ_{MP} around the C_{meso}–C_{phenyl} bond for a series of BODIPY dyes.

	pK_a[a]	θ_{MP}[b] [°]		pK_a[a]	θ_{MP}[b] [°]
3b	2.33	90.0	**15**	1.63	48.3
12b	2.54	90.0	**3c**	2.06	90.0
13b	2.05	65.0	**3d**	0.24	90.0
1d	1.81[c]	54.9	**3e**	2.47	90.0
14	1.71	53.7	**16**	–[d]	89.9
10b	1.70	48.9			

[a] In EtOH/water (1:1); corrected value, see Experimental Section for details. [b] Geometry optimisation method: DFT with B3LYP-631G. [c] In EtOH/water (4:1); corrected values. [d] Too acidic. The compound seems to decompose before an increase in fluorescence can be observerd upon addition of $HClO_4$.

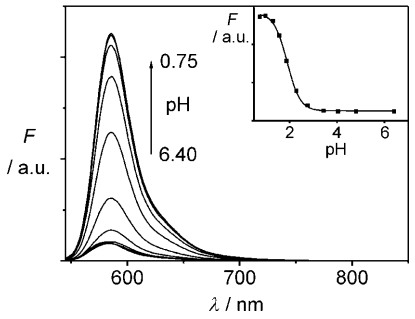

Figure 13. Titration spectra of **1d** with $HClO_4$ in EtOH/H_2O 4:1 v/v.

Conclusion

The synthesis, spectroscopic and theoretical investigation of a new series of red-emissive BODIPY dyes has been presented here. In addition to providing important knowledge on structure–property relationships in BODIPY dyes, the unique electronic and steric effects that can be achieved by adequate substitution of the BODIPY core allowed the obtainment of dyes that perfectly match the spectral range of the most popular rhodamine dyes. In view of their high molar absorption coefficients and fluorescence quantum yields as well as their excellent photostability (e.g., of **1a**,**b**), these dyes can supplement rhodamines for more lipophilic applications such as the doping of polymer beads or membranes. Moreover, with respect to 3,5-diphenyl- or 1,3,5,7-tetraphenyl-BODIPYs (e.g., **5** and **6** in Scheme 2), the series presented here absorbs and emits in the same spectral region while retaining all possibilities for further modification at the 3,5-positions of the BODIPY core. Besides the *meso* position, these are the primary places for further functionalisation of BODIPY dyes. By taking into account the colour rules for 3,5-dimethylaminostyryl extension discussed in the Introduction, BODIPY dyes absorbing at >750 nm might thus be possible. Our studies revealed the importance of electronic effects and the deliberate choice of the position of substitution such that attachment of the DHN units like in **1** and **2** can counterbalance the effect of *meso*-atom exchange. The pH indication features of a series of DMA–BODIPYs and the dependence of the pK_a on the interannular twisting angle impressively show the possibilities of fine-tuning. As previous work on **3b** has shown,[85] these properties can be readily exploited for pH sensing. The transference of the knowledge obtained here to *meso*-phenol-substituted derivatives[76] is expected to offer similar modes of tuning for indicators for the basic pH range.

Experimental Section

General: All syntheses were carried out under an inert atmosphere. Unless otherwise noted, all chemicals and solvents were of commercial reagent grade and used without further purification. Dry dichloromethane was freshly distilled over CaH_2 under nitrogen. Triethylamine was obtained by simple distillation. Dry toluene was distilled from sodium/benzophenone under an inert atmosphere. Column chromatography and TLC were performed using C-200 (Wakogel) and Kieselgel 60F254 (Merck), respectively. ^{1}H NMR spectra were recorded in $CDCl_3$ and using a Bruker 400 MHz spectrometer at room temperature. NMR spectroscopic chemical shifts are expressed relative to the $CHCl_3$ signal at $\delta=$ 7.26 ppm. MALDI-TOF MS and HRMS (FAB) measurements were done at Ehime University, Matsuyama, Japan. All the solvents employed for the spectroscopic measurements were of UV-spectroscopic grade and purchased from Aldrich.

General synthetic procedure for the preparation of 1a, 1c and 1d: 3-Methyl-4,5-dihydro-2*H*-benzo[*e*]isoindole **I**[51] (366 mg, 2 mmol) and an aldehyde (benzaldehyde (127 mg, 1.2 mmol; **1a** and **1c**), 4-(dimethylamino)benzaldehyde (179 mg, 1.2 mmol; **1a** and **1d**)) were dissolved in dry CH_2Cl_2 (100 mL) under nitrogen. One drop of TFA was added, and the solution was stirred at room temperature in the dark for 4 h. Then DDQ (454 mg, 2 mmol) was added, and the mixture was stirred for an additional hour. The reaction mixture was subsequently treated with TEA (3 mL) and $BF_3{\cdot}Et_2O$ (3 mL). After stirring for 30 min, the dark brown solution was washed with water and brine, dried over Na_2SO_4, and concentrated at reduced pressure. The crude product was purified by silica gel column chromatography (elution with 5% ethyl acetate/petroleum ether to obtain **1a**, 7% ethyl acetate/petroleum ether to obtain **1c**, 10% ethyl acetate/petroleum ether to obtain **1d**). The compounds were recrystallised from chloroform/methanol to give **1a** as orange crystals (20% yield), **1c** as red crystals (<1% yield) and **1d** as red needles (15% yield).

Compound 1a: ^{1}H NMR (400 MHz, $CDCl_3$): $\delta=7.88$ (s, 1H), 7.61 (d, $J=$ 7.7 Hz, 2H), 7.36–7.28 (m, 6H), 2.92 (t, $J=7.3$ Hz, 4H), 2.61 (t, $J=$ 7.6 Hz, 4H), 2.59 ppm (s, 6H); HRMS (EI): m/z: calcd for $C_{27}H_{23}N_2F_2B$: 424.1954 $[M]^+$; found: 424.1922 $[M]^+$.

Compound 1c: ^{1}H NMR (500 MHz, $CDCl_3$): $\delta=7.66$ (d, $J=7.2$ Hz, 2H), 7.467 (d, $J=7.0$ Hz, 2H), 7.38–7.33 (m, 7H), 7.18 (t, $J=7.7$ Hz, 2H), 3.01 (t, $J=7.1$ Hz, 4H), 2.94 (t, $J=7.2$ Hz, 4H), 2.63 ppm (s, 6H); HRMS (FAB): m/z: calcd for $C_{33}H_{28}N_2F_2B$: 501.2313 $[M+H]^+$; found: 501.2315 $[M+H]^+$.

Compound 1d: ^{1}H NMR (400 MHz, $CDCl_3$): $\delta=7.10$ (d, $J=7.3$ Hz, 2H), 7.04 (d, $J=8.8$ Hz, 2H), 6.84 (td, $J_1=7.4$ Hz, $J_2=1.2$ Hz, 2H), 6.48 (td, $J_1=7.4$ Hz, $J_2=1.2$ Hz, 2H), 6.29 (d, $J=8.3$ Hz, 2H), 6.07 (d, $J=7.7$ Hz, 2H), 2.85 (s, 6H), 2.81 (t, $J=7.0$ Hz, 4H), 2.62 (s, 6H), 2.47 ppm (t, $J=$ 6.9 Hz, 4H); HRMS (EI): m/z: calcd for $C_{35}H_{32}N_3F_2B$: 543.2657 $[M]^+$; found: 543.2658 $[M]^+$.

Compound 1b: Compound **I** (366 mg, 2 mmol) and acetyl chloride (94.2 mg, 1.2 mmol) were dissolved in dry CH_2Cl_2 (80 mL) under nitrogen, and the solution was heated at reflux in the dark for 6 h. After the mixture was cooled to room temperature, the reaction mixture was treated with TEA (3 mL) and $BF_3{\cdot}Et_2O$ (3 mL). After stirring for another 30 min, the dark brown solution was washed with water and brine, dried over Na_2SO_4, and concentrated at reduced pressure. The crude product was purified by column chromatography (silica gel, 5% ethyl acetate/petroleum ether) and recrystallised from chloroform/methanol to give **1b** as orange crystals (27% yield). ^{1}H NMR (400 MHz, $CDCl_3$): $\delta=7.60$ (d, $J=$ 7.7 Hz, 2H), 7.34–7.23 (m, 6H), 2.85–2.82 (m, 7H), 2.59 (s, 6H), 2.50 ppm (t, $J=7.0$ Hz, 4H); HRMS (EI): m/z: calcd for $C_{28}H_{25}N_2F_2B$: 438.2079 $[M]^+$; found: 438.2079 $[M]^+$.

Compound 2: Compound **I** (366 mg, 2 mmol) and $NaNO_2$ (69 mg, 1 mmol) were stirred in AcOH/Ac_2O (10:4 v/v) at 0°C for half an hour and then at 80°C for another half an hour. The mixture was diluted with cold water and neutralised with NaOH (4M) solution to form solid precipitates. After washing with water and drying, the solid was stirred with TEA (3 mL) and $BF_3{\cdot}Et_2O$ (3 mL) in dry CH_2Cl_2 (100 mL) for 3 h. The dark red solution was washed with water and brine, dried over Na_2SO_4, and concentrated at reduced pressure. The crude product was purified by column chromatography (silica gel, 20% ethyl acetate/petroleum ether) and recrystallised from chloroform/methanol to give **2** as orange crystals (25% yield). ^{1}H NMR (400 MHz, $CDCl_3$): $\delta=7.60$ (d, $J=7.3$ Hz, 2H), 7.32–7.20 (m, 6H), 2.96 (t, $J=7.0$ Hz, 4H), 2.59 (t, $J=7.4$ Hz, 4H), 2.50 ppm (s, 6H); HRMS (EI): m/z: calcd for $C_{26}H_{22}N_3F_2B$: 425.1875 $[M]^+$; found: 425.1875 $[M]^+$.

Crystal structure determination: A single crystal of compound **1a** was selected under a microscope and mounted on a glass fibre. The unit-cell parameters and data were collected using a Bruker Smart Apex CCD diffractometer with graphite-monochromatised $Mo_{K\alpha}$ radiation ($\lambda =$ 0.71073 Å) using the ω–2θ scan mode. The data were corrected for Lorenz and polarisation effects. The structure was solved by direct methods and refined on F^2 by full-matrix least-squares methods using the SHELXTL-2000 program package.[86] CCDC-629010 (**1a**) contains the supplementary crystallographic data for this paper. These data can be obtained free of charge from The Cambridge Crystallographic Data Centre via www.ccdc.cam.ac.uk/data_request/cif.

Steady-state absorption and fluorescence spectroscopy: Steady-state absorption and fluorescence measurements were carried out using a Cary 5000 UV/Vis-NIR spectrophotometer, a Bruins Instruments Omega 10 spectrophotometer, a Spectronics Instrument 8100 spectrofluorometer and a Perkin–Elmer LS50B spectrofluorometer, the latter for fluorescence titrations. For all measurements, the temperature was kept constant at (298 ± 1) K. Unless otherwise noted, only dilute solutions with an absorbance of less then 0.1 at the absorption maximum were used. Fluorescence experiments were performed with a 90° standard geometry, with polarisers set at 54.7° for emission and 0° for excitation. The fluorescence quantum yields (Φ_f) of **1a–d** and **2** were determined relative to rhodamine 101 in ethanol ($\Phi_f = 1.00 \pm 0.02$).[87] By employing the traceably characterised Spectronics Instrument 8100 spectrofluorometer,[88] the uncertainties of measurement were determined to ±5% (for $\Phi_f > 0.2$), ±10% (for $0.2 > \Phi_f > 0.02$) and ±20% (for $0.02 > \Phi_f$).

Time-resolved fluorescence spectroscopy: Fluorescence lifetimes (τ_f) were determined by a unique customised laser-impulse fluorometer with picosecond time resolution, which we have described in earlier publications.[29,89] The fluorescence was collected at right angles (polariser set at 54.7°; monochromator with spectral bandwidths of 4, 8 and 16 nm) and the fluorescence decays were recorded using a modular single-photon timing unit described in ref. [29]. While realising typical instrumental response functions of fwhm of approximately 25–30 ps, the time division was 4.8 ps per channel and the experimental accuracy amounted to ±3 ps, respectively. The laser beam was attenuated using a double-prism attenuator from LTB and typical excitation energies were in the nanowatt to microwatt range (average laser power). The fluorescence lifetime profiles were analysed with a PC using the software package Global Unlimited V2.2 (Laboratory for Fluorescence Dynamics, University of Illinois). The goodness of the fit of the single decays as judged by reduced chi-squared (χ^2_R) and the autocorrelation function $C(j)$ of the residuals was always below $\chi^2_R < 1.2$. For all the dyes, decays were recorded at three different emission wavelengths over the BODIPY-type emission spectrum and analysed globally. Such a global analysis of decays recorded at different emission wavelengths implies that the decay times of the species are linked while the program varies the pre-exponential factors and lifetimes until the changes in the error surface (χ^2 surface) are minimal, that is, convergence is reached. The fitting results are judged for every single decay (local χ^2_R) and for all the decays (global χ^2_R), respectively. The errors for all the global analytical results presented here were below a global $\chi^2_R = 1.2$.

Photostability measurements: Photostability studies were conducted with a customised setup using a 150 W xenon lamp that irradiates a 10 mm cuvette at 560 nm with a slit width of 15 nm. The spot size of the beam focused on the cuvette was 1.5 cm^2. The samples consisted of 2500 μL dye solution, adjusted to optical densities of approximately 0.11 and were exposed for 8 h with an average excitation intensity of 1.1 $mW\,cm^{-2}$. The excitation energy was measured with an Si diode, calibrated by the Physikalisch-Technische Bundesanstalt, to calculate the number of transmitted and absorbed photons, by taking into account the photonic nature of light. On the basis of these results, the decrease of the concentration can be calculated using the Lambert–Beer law.

Measurements of pH: For every step of the pH titration, small amounts of concentrated $HClO_4$ (1, 0.1 and 0.01 M) were added (microliter pipette, Eppendorf) directly to the measurement cuvette, filled up with a solution (2500 μL) containing the dye (approximately 2 μM) in a mixture of EtOH/water (4:1 for **1d**, 1:1 for the other BODIPY derivatives). The $HClO_4$ was added in a small amount of typically 1–2 vol% of these EtOH/water mixtures (2500 μL). The pH was monitored at 298 K using a digital pH meter (WTW pH 537) equipped with a glass electrode (Mettler Toledo InLab 423). Calibration of the instrument was performed with standard aqueous solutions of pH 4.01 and 6.86 from WTW. The measured pH value was corrected by taking into account differences in liquid junction potentials and proton activity coefficients between the solvent mixture of the sample and the aqueous calibration solution according to a procedure described in detail in ref. [90]. pK_a data were determined from at least two replicate measurements.

Computational details: The optimisation of the S_0 ground-state geometries in the gas phase was performed with the density functional theory (DFT) method employing the hybrid functional B3LYP with a 6-31G(d) basis set and energy minimised as implemented in Gaussian 03.[68] The excitation energies and the oscillator strengths were obtained using the time-dependent density functional theory (TD-DFT) method at the TD-B3LYP/6-31G(d) level of theory on the B3LYP/6-31G(d)-optimised S_0 geometry.

Acknowledgements

Financial support from the National Natural Science Foundation of China (nos. 20875043 and 20971066), the Program for New Century Excellent Talents in University (no. NCET-08-0272), the Major State Basic Research Development Program (grant nos. 2006CB806104 and 2007CB925103), the European Commission for a Marie Curie Fellowship and BAM for an Adolf Martens Fellowship (A.B.D.) is highly appreciated.

[1] A. Loudet, K. Burgess, *Chem. Rev.* **2007**, *107*, 4891–4932.
[2] F. López-Arbeloa, J. Banuelos, V. Martinez, T. Arbeloa, I. Lopez-Arbeloa, *Int. Rev. Phys. Chem.* **2005**, *24*, 339–374.
[3] R. Ziessel, G. Ulrich, A. Harriman, *New J. Chem.* **2007**, *31*, 496–501.
[4] G. Ulrich, R. Ziessel, A. Harriman, *Angew. Chem.* **2008**, *120*, 1202–1219; *Angew. Chem. Int. Ed.* **2008**, *47*, 1184–1201.
[5] A. B. Descalzo, H.-J. Xu, Z. Shen, K. Rurack, *Ann. N. Y. Acad. Sci.* **2008**, *1130*, 164–171.
[6] D. L. Marks, R. Bittman, R. E. Pagano, *Histochem. Cell Biol.* **2008**, *130*, 819–832.
[7] Number of hits of articles for the search topic (BODIPY* or boron-dipyrromethen* or boron-dipyrrin*) and (dye* or fluorophor* or chromophor* or label* or probe* or sensor* or stain* or chemosensor* or indicator*) in ISI Web of Science database as of September 5, 2009: 556 (2005 and later), 264 (2000–2004), 147 (1995–1999) and 28 (1994 and before).
[8] A. Ambroise, R. W. Wagner, P. D. Rao, J. A. Riggs, P. Hascoat, J. R. Diers, J. Seth, R. K. Lammi, D. F. Bocian, D. Holten, J. S. Lindsey, *Chem. Mater.* **2001**, *13*, 1023–1034.
[9] H. Röhr, C. Trieflinger, K. Rurack, J. Daub, *Chem. Eur. J.* **2006**, *12*, 689–700.
[10] V. A. Azov, A. Beeby, M. Cacciarini, A. G. Cheetham, F. Diederich, M. Frei, J. K. Gimzewski, V. Gramlich, B. Hecht, B. Jaun, T. Latychevskaia, A. Lieb, Y. Lill, F. Marotti, A. Schlegel, R. R. Schlittler, P. J. Skinner, P. Seiler, Y. Yamakoshi, *Adv. Funct. Mater.* **2006**, *16*, 147–156.
[11] A. Harriman, G. Izzet, R. Ziessel, *J. Am. Chem. Soc.* **2006**, *128*, 10868–10875.
[12] L. Bonardi, H. Kanaan, F. Camerel, P. Jolinat, P. Retailleau, R. Ziessel, *Adv. Funct. Mater.* **2008**, *18*, 401–413.
[13] M. Tomasulo, E. Deniz, R. J. Alvarado, F. M. Raymo, *J. Phys. Chem. C* **2008**, *112*, 8038–8045.
[14] W. Qin, T. Rohand, W. Dehaen, J. N. Clifford, K. Driesen, D. Beljonne, B. Van Averbeke, M. Van der Auweraer, N. Boens, *J. Phys. Chem. A* **2007**, *111*, 8588–8597.

[15] A. Loudet, R. Bandichhor, K. Burgess, A. Palma, S. O. McDonnell, M. J. Hall, D. F. O'Shea, *Org. Lett.* **2008**, *10*, 4771–4774.
[16] A. Wakamiya, N. Sugita, S. Yamaguchi, *Chem. Lett.* **2008**, *37*, 1094–1095.
[17] Y. Cakmak, E. U. Akkaya, *Org. Lett.* **2009**, *11*, 85–88.
[18] P. A. Bouit, K. Kamada, P. Feneyrou, G. Berginc, L. Toupet, O. Maury, C. Androud, *Adv. Mater.* **2009**, *21*, 1151–1154.
[19] A. Burghart, H. Kim, M. B. Welch, L. H. Thoresen, J. Reibenspies, K. Burgess, *J. Org. Chem.* **1999**, *64*, 7813–7819.
[20] J. Chen, A. Burghart, A. Derecskei-Kovacs, K. Burgess, *J. Org. Chem.* **2000**, *65*, 2900–2906.
[21] B. P. Wittmershaus, J. J. Skibicki, J. B. McLafferty, Y.-Z. Zhang, S. Swan, *J. Fluoresc.* **2001**, *11*, 119–128.
[22] J. Killoran, L. Allen, J. F. Gallagher, W. M. Gallagherb, D. F. O'Shea, *Chem. Commun.* **2002**, 1862–1863.
[23] Y. Mei, P. A. Bentley, W. Wang, *Tetrahedron Lett.* **2006**, *47*, 2447–2449.
[24] W. Zhao, E. M. Carreira, *Angew. Chem.* **2005**, *117*, 1705–1707; *Angew. Chem. Int. Ed.* **2005**, *44*, 1677–1679.
[25] G. Sathyamoorthi, J. H. Boyer, T. H. Allik, S. Chandra, *Heteroat. Chem.* **1994**, *5*, 403–407.
[26] G. Jones II, S. Kumar, O. Klueva, D. Pacheco, *J. Phys. Chem. A* **2003**, *107*, 8429–8434.
[27] K. Umezawa, Y. Nakamura, H. Makino, D. Citterio, K. Suzuki, *J. Am. Chem. Soc.* **2008**, *130*, 1550–1551.
[28] M. Wada, S. Ito, H. Uno, T. Murashima, N. Ono, T. Urano, Y. Urano, *Tetrahedron Lett.* **2001**, *42*, 6711–6713.
[29] Z. Shen, H. Röhr, K. Rurack, H. Uno, M. Spieles, B. Schulz, G. Reck, N. Ono, *Chem. Eur. J.* **2004**, *10*, 4853–4871.
[30] A. B. Descalzo, H.-J. Xu, Z.-L. Xue, K. Hoffmann, Z. Shen, M. G. Weller, X.-Z. You, K. Rurack, *Org. Lett.* **2008**, *10*, 1581–1584.
[31] K. Rurack, M. Kollmannsberger, J. Daub, *Angew. Chem.* **2001**, *113*, 396–399; *Angew. Chem. Int. Ed.* **2001**, *40*, 385–387.
[32] K. Rurack, M. Kollmannsberger, J. Daub, *New J. Chem.* **2001**, *25*, 289–292.
[33] A. Coskun, E. Deniz, E. U. Akkaya, *Org. Lett.* **2005**, *7*, 5187–5189.
[34] A. Coskun, E. U. Akkaya, *J. Am. Chem. Soc.* **2005**, *127*, 10464–10465.
[35] Y.-H. Yu, A. B. Descalzo, Z. Shen, H. Röhr, Q. Liu, Y.-W. Wang, M. Spieles, Y.-Z. Li, K. Rurack, X.-Z. You, *Chem. Asian J.* **2006**, *1*, 176–187.
[36] S. Atilgan, Z. Ekmekci, A. L. Dogan, D. Guc, E. U. Akkaya, *Chem. Commun.* **2006**, 4398–4400.
[37] Z. Dost, S. Atilgan, E. U. Akkaya, *Tetrahedron* **2006**, *62*, 8484–8488.
[38] A. Coskun, E. U. Akkaya, *J. Am. Chem. Soc.* **2006**, *128*, 14474–14475.
[39] Whereas most cyanines and rhodamines are intrinsically positively charged, for fluoresceins, only the negatively charged dianion form is highly fluorescent. See, H. Diehl, R. Markuszewski, *Talanta* **1989**, *36*, 416–418.
[40] R. Méallet-Renault, R. Pansu, S. Amigoni-Gerbier, C. Larpent, *Chem. Commun.* **2004**, 2344–2345.
[41] S. De, D. H. Robinson, *AAPS PharmSciTech* **2005**, *6*, 53.
[42] A. Tronin, T. Xu, J. K. Blasie, *Langmuir* **2005**, *21*, 7760–7767.
[43] T. Yogo, Y. Urano, A. Mizushima, H. Sunahara, T. Inoue, K. Hirose, M. Iino, K. Kikuchi, T. Nagano, *Proc. Natl. Acad. Sci. USA* **2008**, *105*, 28–32.
[44] R. Ziessel, C. Goze, G. Ulrich, *Synthesis* **2007**, 936–949.
[45] K. Rurack, M. Kollmannsberger, U. Resch-Genger, J. Daub, *J. Am. Chem. Soc.* **2000**, *122*, 968–969.
[46] K. Rurack, U. Resch-Genger, *Chem. Soc. Rev.* **2002**, *31*, 116–127.
[47] E. Deniz, G. C. Isbasar, Ö. A. Bozdemir, L. T. Yildirim, A. Siemiarczuk, E. U. Akkaya, *Org. Lett.* **2008**, *10*, 3401–3403.
[48] Q. Zheng, G. Xu, P. N. Prasad, *Chem. Eur. J.* **2008**, *14*, 5812–5819.
[49] R. Ziessel, G. Ulrich, A. Harriman, M. A. H. Alamiry, B. Stewart, P. Retailleau, *Chem. Eur. J.* **2009**, *15*, 1359–1369.
[50] These rules of thumb only pertain to the absorption maxima since only the ground-state dipole moment of all the BODIPY dyes listed in the scheme is sufficiently small so that solvent-polarity-dependent shifts can be neglected. Moreover, for **4** and **5**, the 4-iodophenyl substituent in the *meso* position has virtually no influence on the BODIPY-centred $S_1 \leftarrow S_0$ transition. The same accounts for the *meso*-hydroxyquinoline groups in **8** and **11** because of their perpendicular orientation. See the original publications for detailed discussions of these compounds.
[51] J. M. Manley, T. J. Roper, T. D. Lash, *J. Org. Chem.* **2005**, *70*, 874–891.
[52] M. Kollmannsberger, T. Gareis, S. Heinl, J. Breu, J. Daub, *Angew. Chem.* **1997**, *109*, 1391–1393; *Angew. Chem. Int. Ed. Engl.* **1997**, *36*, 1333–1335.
[53] J. Chen, J. Reibenspies, A. Derecskei-Kovacs, K. Burgess, *Chem. Commun.* **1999**, 2501–2502.
[54] A. G. Montalban, A. J. Herrera, J. Johannsen, J. Beck, T. Godet, M. Vrettou, A. J. P. White, D. J. Williams, *Tetrahedron Lett.* **2002**, *43*, 1751–1753.
[55] B. Herradon, A. Chana, M. Alonso, F. Amat-Guerri, M. Liras, M. A. Maestro, *J. Mol. Struct.* **2004**, *697*, 29–40.
[56] R. Ziessel, L. Bonardi, G. Ulrich, *Dalton Trans.* **2006**, 2913–2918.
[57] R. Ziessel, L. Bonardi, P. Retailleau, G. Ulrich, *J. Org. Chem.* **2006**, *71*, 3093–3102.
[58] Y.-H. Yu, Z. Shen, H.-Y. Xu, Y.-W. Wang, T. Okujima, N. Ono, Y.-Z. Li, X.-Z. You, *J. Mol. Struct.* **2007**, *827*, 130–136.
[59] A. Cui, X. Peng, J. Fan, X. Chen, Y. Wu, B. Guo, *J. Photochem. Photobiol. A* **2007**, *186*, 85–92.
[60] Y.-W. Wang, M. Li, Z. Shen, X.-Z. You, *Chin. J. Inorg. Chem.* **2008**, *24*, 1247–1252.
[61] Because of these findings and the inherent uncertainties that would accompany a deconvolution of the highly overlapping bands, we refrained from a derivation of global-band or single-transition oscillator strengths from solution absorption spectra.
[62] Derivative spectroscopy is well suited for analysing shoulders and overlapping bands, see, for example, H.-H. Perkampus, *UV-VIS Spectroscopy and Its Applications*, Springer, Berlin, **1992**, pp. 88–94.
[63] The fluorescence excitation spectra are independent of emission wavelength and basically match the absorption spectra.
[64] Excluding the dependence of k_r on the emission-band position by consideration of the reduced radiative rate constants κ_f yields an even better agreement. See Table S2 in the Supporting Information.
[65] M. Kollmannsberger, K. Rurack, U. Resch-Genger, J. Daub, *J. Phys. Chem. A* **1998**, *102*, 10211–10220.
[66] $r=(F_{VV}-F_{VH})/(F_{VV}+2F_{VH})$ in which r=anisotropy, F=fluorescence intensity and subscripts V and H represent vertically and horizontally aligned polarisers.
[67] The higher transitions (<400 nm) are presumably mixed and involve various molecular orbitals localised asymmetrically on the dihydronaphthalene-BODIPY fragment. Since these transitions are not relevant within the context of this manuscript, no further assignment was attempted.
[68] Gaussian 03, Revision D.01, M. J. Frisch, G. W. Trucks, H. B. Schlegel, G. E. Scuseria, M. A. Robb, J. R. Cheeseman, J. A. Montgomery, Jr., T. Vreven, K. N. Kudin, J. C. Burant, J. M. Millam, S. S. Iyengar, J. Tomasi, V. Barone, B. Mennucci, M. Cossi, G. Scalmani, N. Rega, G. A. Petersson, H. Nakatsuji, M. Hada, M. Ehara, K. Toyota, R. Fukuda, J. Hasegawa, M. Ishida, T. Nakajima, Y. Honda, O. Kitao, H. Nakai, M. Klene, X. Li, J. E. Knox, H. P. Hratchian, J. B. Cross, V. Bakken, C. Adamo, J. Jaramillo, R. Gomperts, R. E. Stratmann, O. Yazyev, A. J. Austin, R. Cammi, C. Pomelli, J. W. Ochterski, P. Y. Ayala, K. Morokuma, G. A. Voth, P. Salvador, J. J. Dannenberg, V. G. Zakrzewski, S. Dapprich, A. D. Daniels, M. C. Strain, O. Farkas, D. K. Malick, A. D. Rabuck, K. Raghavachari, J. B. Foresman, J. V. Ortiz, Q. Cui, A. G. Baboul, S. Clifford, J. Cioslowski, B. B. Stefanov, G. Liu, A. Liashenko, P. Piskorz, I. Komaromi, R. L. Martin, D. J. Fox, T. Keith, M. A. Al-Laham, C. Y. Peng, A. Nanayakkara, M. Challacombe, P. M. W. Gill, B. Johnson, W. Chen, M. W. Wong, C. Gonzalez, J. A. Pople, Gaussian, Inc., Wallingford CT, **2004**.
[69] To find the best compromise between reasonable processing times and sufficiently accurate modelling for our present purposes, we

first performed a theoretical treatment of **1a** with the B3LYP functional and different basis sets (6-31G, 6-31G(d), and 6-31G(d,p)) and compared key structural parameters thus obtained with experimental results from X-ray analysis (see Table S3 in the Supporting Information for an overview). These trials revealed good agreement of the experimental results with the results obtained for the 6-31G(d) and 6-31G(d,p) basis sets and that the latter do not show significant differences. The 6-31G(d) basis set was thus chosen here.

[70] For **1c**,**d**, the hypothetical kinked–parallel "butterfly-like" conformation (see Figure 6B) was also considered as a possible starting structure for the optimisation. These "out-of-plane" structures also converged (Figure S3 in the Supporting Information), however, and as would be expected, they are clearly disfavoured by 45.3 and 32.1 kJ mol^{-1} with respect to the most stable structure for **1c** and **1d**, respectively. This is reflected in the largest θ_{PP} found here, 29.4 and 29.9° for **1c** and **1d**, respectively.

[71] Commonly, the influence of the *meso* substituent is mostly of inductive nature because, upon electronic excitation, the charge redistribution in the indacene core of BODIPY dyes usually results in an increase of the electronic density at C_{meso} upon going from the highest-occupied to the lowest-unoccupied BODIPY-centred MO.[35] As a consequence, electron-donor substituents like anilines attached to the *meso* position destabilise these features, thereby leading to a larger energy gap for the BODIPY-centred optical transitions and hypsochromic shifts in absorption.[30,35]

[72] A. A. Gorman, I. Hamblett, T. A. King, M. D. Rahn, *J. Photochem. Photobiol. A* **2000**, *130*, 127–132.

[73] J. Bañuelos Prieto, F. López Arbeloa, V. Martínez Martínez, T. Arbeloa López, I. López Arbeloa, *Phys. Chem. Chem. Phys.* **2004**, *6*, 4247–4253.

[74] J. Tomasi, M. Persico, *Chem. Rev.* **1994**, *94*, 2027–2094.

[75] A direct comparison of **1a–c** versus **5b** and **6** versus **5b** is, however, complicated because of the mixed nature of the lowest-energy transitions in the title dyes and the pure HOMO–LUMO character of the only low-lying $S_1 \leftarrow S_0$ transition in the model dyes.

[76] T. Gareis, C. Huber, O. S. Wolfbeis, J. Daub, *Chem. Commun.* **1997**, 1717–1718.

[77] K. Rurack, J. Daub, M. Kollmannsberger, unpublished results.

[78] J. L. Bricks, A. Kovalchuk, C. Trieflinger, M. Nofz, M. Büschel, A. I. Tolmachev, J. Daub, K. Rurack, *J. Am. Chem. Soc.* **2005**, *127*, 13522–13529.

[79] The pK_a data obtained by fluorescence agree well with those measured by absorption for all the dyes investigated here (±0.04 units). However, in contrast to the strong increase in fluorescence, protonation is only visible by a shift of the main BODIPY band of about 3 nm (**3b**) to 13 nm (**10b**) in absorption.

[80] J. W. Eastes, M. H. Aldridge, M. J. Kamlet, *J. Chem. Soc. B* **1969**, 922–928.

[81] D. J. Cowley, E. O'Kane, R. S. J. Todd, *J. Chem. Soc. Perkin Trans. 2* **1991**, 1495–1500.

[82] With an ethylene bridge between N and S/O, through-space and through-bond inductive effects might both play a role.

[83] B. García-Acosta, R. Martínez-Máñez, F. Sancenón, J. Soto, K. Rurack, M. Spieles, E. García-Breijo, L. Gil, *Inorg. Chem.* **2007**, *46*, 3123–3135.

[84] Note: The unexpectedly high pK_a together with recent observations by Burdette and co-workers (D. P. Kennedy, C. D. Incarvito, S. C. Burdette, *Inorg. Chem.* published on the web January 4, 2010, DOI: 10.1021/ic901182c) suggest that the fluorescence changes of **3e** in aqueous solution in the presence of Fe^{3+} reported in ref. [78] are not due to the ascribed binding of the metal ion but to protonation by residual H^+ at the considerably low buffer concentrations employed in that study.

[85] T. Werner, C. Huber, S. Heinl, M. Kollmannsberger, J. Daub, O. S. Wolfbeis, *Fresenius J. Anal. Chem.* **1997**, *359*, 150–154.

[86] SMART, SAINT, SADABS and SHELXTL, Bruker AXS Inc., Madison, **2000**.

[87] D. F. Eaton, *Pure Appl. Chem.* **1988**, *60*, 1107–1114.

[88] U. Resch-Genger, D. Pfeifer, C. Monte, W. Pilz, A. Hoffmann, M. Spieles, K. Rurack, J. Hollandt, D. Taubert, B. Schönenberger, P. Nording, *J. Fluoresc.* **2005**, *15*, 315–336.

[89] U. Resch, K. Rurack, *Proc. SPIE-Int. Soc. Opt. Eng.* **1997**, *3105*, 96–103.

[90] M. Maus, K. Rurack, *New J. Chem.* **2000**, *24*, 677–686.

Received: September 14, 2009
Revised: November 25, 2009
Published online: January 26, 2010

